

Article

Integration of Complexed Caffeic Acid into Poly(Lactic Acid)-Based Biopolymer Blends by Supercritical CO₂-Assisted Impregnation and Foaming: Processing, Structural and Thermal Characterization

Patricia Rivera ^{1,2} , Alejandra Torres ^{1,*}, Miguel Pacheco ^{1,2}, Julio Romero ², Marina P. Arrieta ^{3,4,*} , Francisco Rodríguez-Mercado ¹  and Julio Bruna ¹ 

- ¹ Packaging Innovation Center (LABEN), Faculty of Technology, Center for the Development of Nanoscience and Nanotechnology (CEDENNA), University of Santiago de Chile (USACH), Santiago 9170201, Chile; patricia.rivera.f@usach.cl (P.R.); miguel.pacheco.a@usach.cl (M.P.); francisco.rodriguez.m@usach.cl (F.R.-M.); julio.bruna@usach.cl (J.B.)
- ² Laboratory of Membrane Separation Processes (LabProSeM), Department of Chemical Engineering, Engineering Faculty, University of Santiago de Chile, Santiago 9170201, Chile; julio.romero@usach.cl
- ³ Departamento de Ingeniería Química Industrial y del Medio Ambiente, Escuela Técnica Superior de Ingenieros Industriales, Universidad Politécnica de Madrid (ETSII-UPM), Calle José Gutiérrez Abascal 2, 28006 Madrid, Spain
- ⁴ Grupo de Investigación, Polímeros, Caracterización y Aplicaciones (POLCA), 28006 Madrid, Spain
- * Correspondence: alejandra.torresm@usach.cl (A.T.); m.arrieta@upm.es (M.P.A.)

Abstract: Conventional techniques for incorporating active ingredients into polymeric matrices are accompanied by certain disadvantages, primarily attributable to the inherent characteristics of the active ingredient itself, including its sensitivity to temperature. A potential solution to these challenges lies in the utilization of supercritical carbon dioxide (scCO₂) for the formation of polymeric foam and the incorporation of active ingredients, in conjunction with the encapsulation of inclusion complexes (ICs), to ensure physical stability and augmented bioactivity. The objective of this study was to assess the impact of IC impregnation and subsequent foam formation on PLA films and PLA/PBAT blends that had been previously impregnated. The study's methodology encompassed the formation and characterization of ICs with caffeic acid (CA) and β -cyclodextrin (β -CD), along with the thermal, structural, and morphological properties of the resulting materials. Higher incorporation of impregnated IC into the PLA(42)/PBAT(58) blend was observed at 12 MPa pressure and a depressurization rate of 1 MPa/min. The presence of IC, in addition to a lower rate of expansion, contributed to the formation of homogeneous cells with a size range of 4–44 μ m. On the other hand, the incorporation of IC caused a decrease in the crystallinity of the PLA fraction due to the interaction of the complex with the polymer. This study makes a significant contribution to the advancement of knowledge on the incorporation of compounds encapsulated in β -CD by scCO₂, as well as to the development of active materials with potential applications in food packaging.

Keywords: active supercritical foams; supercritical carbon dioxide; inclusion complex; food packaging



Academic Editor: Francesco Trotta

Received: 5 January 2025

Revised: 8 March 2025

Accepted: 11 March 2025

Published: 18 March 2025

Citation: Rivera, P.; Torres, A.; Pacheco, M.; Romero, J.; Arrieta, M.P.; Rodríguez-Mercado, F.; Bruna, J. Integration of Complexed Caffeic Acid into Poly(Lactic Acid)-Based Biopolymer Blends by Supercritical CO₂-Assisted Impregnation and Foaming: Processing, Structural and Thermal Characterization. *Polymers* **2025**, *17*, 803. <https://doi.org/10.3390/polym17060803>

Copyright: © 2025 by the authors. Licensee MDPI, Basel, Switzerland. This article is an open access article distributed under the terms and conditions of the Creative Commons Attribution (CC BY) license (<https://creativecommons.org/licenses/by/4.0/>).

1. Introduction

Polymeric foams are porous microstructures and are defined as a two-phase gas-polymer system [1]. Among the polymers used are expanded polystyrene (EPS) and

expanded polyethylene (EPE) [2–4], as these possess good barrier properties, which help preserve the freshness of perishable products such as fruits, seafood, vegetables, and some cheeses. However, many of these containers are used only once before being discarded. Because they are not biodegradable, they must be recycled or incinerated, which generates a high volume of waste in landfills and causes significant environmental impact [5]. Based on this, some eco-friendly alternatives have been reported, such as starch, cellulose, and poly lactic acid (PLA) foams [6–8]. Among the alternatives, PLA is a bio-based, biodegradable, and biocompatible polymer with properties that make it a potential replacement for polystyrene (PS) [9]. In addition, PLA requires 25–55% less energy to produce than petroleum-derived polymers [10]. Although these polymers may have similar properties to those used commercially, they present certain processing difficulties, so the search for strategies such as copolymerization, development of bionanocomposites, and polymer blending has been resorted to, obtaining products like those on the market and with a low environmental impact [11].

Among the main requirements for the foaming process to occur effectively is to melt or plasticize a polymer matrix to allow the diffusion of gases within its structure [12]. In this sense, these materials can be obtained mainly by using chemical blowing agents, such as chlorofluorocarbons (CFCs), for which alternatives have been sought, including the use of supercritical fluids, due to the growing emphasis on environmental protection [13]. A pure component is in a supercritical state if its temperature and pressure are higher than critical values, allowing it to diffuse solids as a gas and dissolve materials as a liquid. These include carbon dioxide (CO₂) and nitrogen (N₂). scCO₂ is characterized by its relatively low critical temperature and pressure, cost-effectiveness, biocompatibility with the human body (non-toxicity), and current classification by the U.S. Food and Drug Administration (FDA) as a safe biomaterial (GRAS) [14]. CO₂ can be used in many fields, such as compound preparation and oil field development [15,16]. Such conditions make this method more environmentally friendly, in addition to avoiding the formation of residues after foaming [12]. In this way, Chang and co-workers prepared blends of thermoplastic starch (TPS), silane A (SA), and PBAT for the development of foams at pressures of 17 and 23.8 MPa [17]. In another work, Faba et al. developed PLA foams loaded with carvacrol cocrystals by means of supercritical CO₂, which showed microcellular sizes and a modulated release by the cocrystal incorporation [18].

Food preservation has been widely studied due to its enormous relevance in social and economic development on a global scale. In recent years, several technologies have emerged to increase and improve food preservation, among them active packaging, in which the packaging interacts positively with the product, prolonging its shelf life thanks to the action of an active agent, which can be incorporated into the packaging material or be part of the polymeric packaging. The economic viability and the environmental benefits of active packaging compared to commercial packaging have been discussed in literature [19,20]. Phenolic acids are found in various foods of plant origin. They are formed by the substitution of hydrogen atoms in a benzene ring by a carboxyl group and a hydroxyl group [21]. They stand out for their antioxidant activity due to radical scavenging by hydrogen atom donation. In this context, 3,4-dihydroxycinnamic acid, also known as caffeic acid (CA), is a notable phenolic compound [22]. CA is a prevalent compound in a wide variety of plants, fruits, and propolis samples [23]. It exhibits diverse bioactivities, such as antiviral, antimicrobial, and anti-inflammatory [24–26]. In addition to its use as a crosslinker for materials such as chitosan, the study by Pei et al. using PLA films with CA immobilized on chitosan effectively decreased the browning, respiration rate, and microorganism-induced deterioration of *Agaricus Bisporus*, thus reducing oxidative damage and delaying aging [27]. Meanwhile, Luzi and co-workers, by casting process,

developed active films of 5 and 15 wt% poly (vinyl alcohol-co-ethylene) (EVOH), obtaining higher thermal stability due to the addition of CA [23].

Recent studies have suggested that the use of cyclodextrins (CDs) can enhance the functionalities of the active, such as increasing the antioxidant activity of an active compound. This is achieved by including the active in its truncated conical form, which has a hydrophilic surface and a hydrophobic cavity [28]. CDs are cyclic oligosaccharides of glucose units linked by an α -(1,4)-glucosidic linkage [29]. In addition, its use as a molecular inclusion technique has been shown to improve chemical stability and provide controlled release, which could allow the development of packaging with continuous and prolonged diffusion, as well as reduce or avoid certain preservatives [30–32]. On the other hand, an increase in the bioactivity of actives has also been found, which could be crucial for the development of active packaging in which the active does not meet the required antioxidant power or in which the active compound incorporated into the material is low [33–35].

Based on this, this work aims to encapsulate CA in a β -cyclodextrin by molecular inclusion, as well as to evaluate the effect of the incorporation of inclusion complexes (β -cyclodextrin/caffeic acid) in PLA and PLA/PBAT mixtures by serial impregnation and supercritical foaming. The study focuses on evaluating the effect of the structure of the developed materials on the structural and morphological thermal properties.

2. Materials and Methods

2.1. Materials

Two commercial PLA/PBAT blends (BASF, Ludwigshafen, Germany), one composed of 42% PLA and 58% PBAT (trade name: Ecovio[®] F2224) [36] and the other with a composition of 4% PLA, 84% PBAT, and 12% inert particles/additives (trade name: Ecovio[®] F23B1) [37], were supplied by Entec Polymers, Chile (Santiago, Chile). Poly (lactic acid) (PLA) 2003D (specific gravity 1.24; MFR g/10 min) was purchased from Natureworks[®] Co (Minnetonka, MN, USA). Carbon dioxide (99.9% purity) was obtained from Linde (Santiago, Chile). Caffeic acid (CA) ($\geq 98\%$ HPLC) and 2,2-diphenyl-1-picrylhydrazyl (DPPH) were obtained from Sigma-Aldrich (Madrid, Spain). β -cyclodextrin ($\geq 98\%$) was obtained from Merck (Darmstadt, Germany). Chromatographic-grade acetonitrile, absolute ethanol, and other analytical-grade reagents from Merck S.A. (Darmstadt, Germany).

2.2. Formation of Inclusion Complexes (IC) Based on β -CD/CA

The IC was prepared according to the coprecipitation method previously reported with some modifications [38]. For this, (5 g/0.044 mol) of β -CD was added slowly to 50 mL of ethanol/water aqueous solution in a 1:2 ratio while this was kept stirring at 50 °C for 2.5 h and 270 rpm on a magnetic stirrer with a thermocouple attached. Pure caffeic acid (0.7936 g/0.044 mol) was then added in a 1:1 molar ratio in an amber flask to protect it from possible degradation by light. The mixture was stirred with a magnetic stirrer for 30 min at 50 °C, then it was cooled to room temperature for 1 h and after that time it was refrigerated for 24 h to favor the precipitation of the inclusion complexes. The sample was then filtered using filter paper and washed numerous times with 10% (*v/v*) ethanol to remove any possible free CA from the precipitate. Finally, the recovered solid phase was dried in a CoolSafe 55-4 Pro freeze dryer (Labogene, Lillerød, Denmark). The inclusion complex was stored in hermetic amber vials at room temperature until further characterization.

2.3. PLA and PLA/PBAT Films Preparation by Extrusion Process

The plastic films were obtained by subjecting various polymer resins to a drying process at 60 °C for 24 h and a melt-extrusion process using a Scientific Labtech[®] LTE20 twin-screw extruder (Praksa, Muang, Samutprakarn, Thailand) located at the Packaging

Innovation Center (LABEN-Chile) of the University of Santiago de Chile. Extruder temperature profiles were maintained at 185–195 °C [39] for PLA films and 170–195 °C for PLA/PBAT blends [40]. The screw speed was set at 42 rpm, and a chill roll was used at 0.9 rpm. Films with thicknesses between 500 and 600 µm were obtained and later cut into 4 × 1.5 cm pieces, whose mass and thickness were measured and then stored in a desiccator.

2.4. Supercritical Impregnation of Inclusion Complex

The initial phase of material processing, encompassing impregnation experiments, was conducted at the Membrane Separation Processes Laboratory (LabProSem) within the Department of Chemical Engineering and Bioprocessing at the University of Santiago de Chile. PLA and PLA/PBAT films developed by the process described in Section 2.3 were processed by supercritical impregnation to incorporate the inclusion complex. The impregnation process (Figure 1) was conducted within a high-pressure cell having a volume of 100 mL and maintained at a constant temperature of 40 °C. The thermostatic resistance surrounding the cell ensured the temperature was consistently regulated throughout the process [39]. CO₂ was loaded into the system employing an ISCO 500D syringe pump (Lincoln, NE, USA), operated at a constant pressure regime during each impregnation cycle.

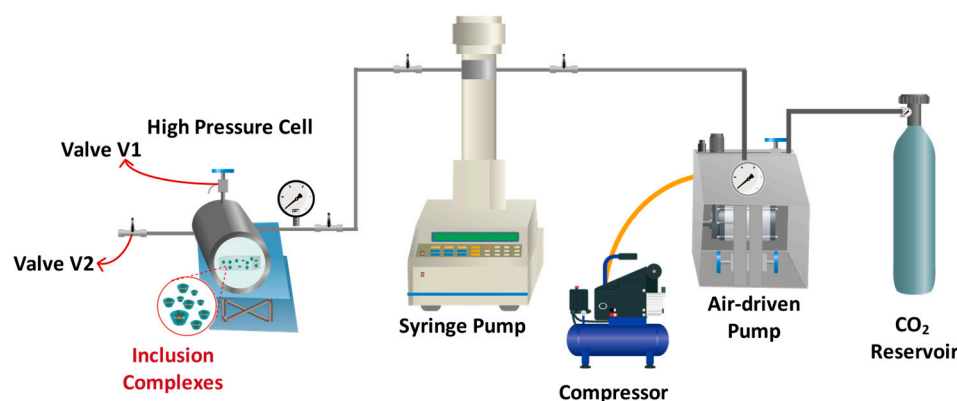


Figure 1. Outline of the experimental setup used for sequential supercritical impregnation and foaming processes.

The impregnation experiments were carried out by loading a quantity of IC equivalent to 10 mg of caffeic acid (337 mg IC) in a high-pressure cell to ensure the saturation condition of the impregnation phase, as used for films containing only pure CA, as reported in previous work [41], since these were considered the best operating conditions obtained for pure CA impregnations. For this, five samples of material with a surface area of 6 cm² each, with a thickness between 500 and 600 µm, were placed in the high-pressure cell, with a vial containing the amount of IC mentioned above. The supercritical impregnation series were carried out at pressures of 12 or 15 MPa at a constant temperature of 40 °C for 3 h to reach equilibrium conditions. After this time, the system was depressurized at 0.1 or 1 MPa/min with a micrometer valve (V1) to characterize and quantify the amount of impregnated active. The operating conditions are described in Table 1. It should be noted that, for each impregnation condition, the tests were performed in duplicate.

Table 1. Conditions for supercritical impregnation of the inclusion complex (IC) in the different films.

Sample	Pressure [MPa]	Depressurization Rate [MPa/min]	Cosolvent Concentration [wt%]
PLA/IC	15	1	0; 5
PLA(42)/PBAT (58)/IC	12	1	0; 5
PLA(4)/PBAT(84)/IC	12	0.1	0; 5

2.5. Supercritical Foaming of PLA and Blends

As delineated in Section 2.4, the impregnated materials underwent a supercritical foaming process following impregnation. The foams derived from PLA and PLA/PBAT blends were produced from materials that had previously undergone impregnation in the presence of a co-solvent. As illustrated in Figure 1, the foaming process was conducted. The samples were placed within the high-pressure cell, and CO₂ was introduced into the system, which was maintained at a constant pressure during the supercritical foaming process. The temperature within the high-pressure cell was regulated by a thermocouple attached to the cell. The supercritical foaming process was conducted at temperatures of 130 °C and pressures ranging from 15 to 25 MPa. The samples were maintained under these conditions for a duration of approximately 25 to 30 min. Subsequently, the CO₂ was expeditiously released at a depressurization rate of 60 MPa/min [39,42] via valve V2 and the samples were stabilized by an air-conditioned cooling system. The foams produced in these experiments were subsequently stored in a desiccator until the stage of characterization. These experiments were performed in duplicate for each condition.

2.6. Encapsulation Efficiency

The amount of caffeic acid trapped in the inclusion complex was determined according to the method proposed by Muñoz et al. [38], with some modifications. The active compound was extracted from 2 mg IC with ethanol (20 mL) in hermetically sealed vials using an incubator shaker IST-4075 (Jeio Tech, Daejeon, Republic of Korea) at 150 rpm and 25 °C for 24 h. The insoluble phase (β -cyclodextrin) was separated by centrifugation, and the supernatant was analyzed spectrophotometrically with UV-1601 Rayleigh (BFRL, Beijing, China) at a wavelength of 242 nm.

The compound was quantified using a previously established calibration curve with different solutions of caffeic acid in ethanol with concentrations ranging from 0 to 30 ppm ($R^2 = 0.99$). From this analysis, the efficiency (EE) was calculated using Equation (1):

$$EE [\%] = \frac{\text{Release CA content}}{\text{Theoretical CA content}} * 100 \quad (1)$$

2.7. Quantification of Active Agent in Impregnated Films

To determine the amount of caffeic acid present in the films and foams, the Folin-Ciocalteu method reported by [43] was used with some modifications. A sample of film or foam was cut into small pieces and placed in a 25 mL amber volumetric flask to protect it from light and possible degradation. A mixture of 1 mL of Folin-Ciocalteu reagent and distilled water was then added and shaken for 2 min. Then 4 mL of sodium carbonate at 2% *w/w* was added, and the solution was made up with distilled water. The samples were measured by UV-visible spectrophotometry (UV 1601, Rayleigh) at 760 nm. The time was determined by the time taken for the samples to reach equilibrium concentration. The content of total phenols was determined by means of a calibration curve with the concentration of caffeic acid. For this purpose, a stock solution of 200 mg/L was prepared and diluted to concentrations in the range of 0.08–1.8 mg/L. The measurements were performed in duplicate and expressed as mg of caffeic acid per mg of pure material (film or foam).

2.8. Characterization of Inclusion Complexes and Materials Obtained (Films and Foams)

2.8.1. Nuclear Magnetic Resonance (NMR)

¹H NMR spectra were recorded for β -cyclodextrin and the inclusion complex dissolved in D₂O using a Varian Mercury 400 MHz spectrometer. Chemical shifts were measured relative to the peak at 4.80 ppm, due to the solvent (D₂O) [44]. The ¹H NMR chemical shifts

for the inclusion complex and β -cyclodextrin were determined. The difference in chemical shift value was considered by Equation (2), where δ_{free} is the chemical shift of the pure component and δ_{complex} is the chemical shift of the complex [45].

$$\Delta\delta = \delta_{\text{complex}} - \delta_{\text{free}} \quad (2)$$

2.8.2. Attenuated Total Reflectance Fourier Transforms Infrared (ATR-FTIR) Spectroscopy

The FTIR spectra of β -CD, CA, and IC were performed using potassium bromide (KBr) pellets, while the materials obtained (films and foams) were obtained by direct contact of a piece of material. An ALPHA spectrometer Platinum (Bruker, Billerica, MA, USA) equipped with an attenuated total reflection (ATR) diamond crystal accessory was employed for this purpose. The spectrometer employed the OPUS v7 software suite, which was configured to perform 64 scans per specimen within a wavelength range spanning from 400 to 4000 cm^{-1} .

2.8.3. Morphological Properties

The morphologies of the different foam samples were analyzed by scanning electron microscopy (SEM) using a Jeol JSM-5410 scanning microscope (Jeol, Shanghai, China) with accelerating voltage at 20 kV. Cell size was measured using ImageJ v1.54g software and was obtained by measuring the maximum diameter of each cell. To determine the cell size distribution, the size of at least 75 cells in the central part of the cross section of the cryofractured foam sample was considered.

The bulk density (kg/m^3) of the pre-foamed (ρ_p) and post-foamed (ρ_f) samples was determined using a pycnometer by the water displacement method according to ASTM D792-20 [46,47]. Cell densities (NC) were calculated using Equation (3).

$$\text{NC} = \frac{\left(1 - \frac{\rho_f}{\rho_p}\right)}{(10^{-4} * d^3)} \quad (3)$$

On the other hand, the expansion coefficient (ER) of the foamed samples was obtained using Equation (4) [42]:

$$\text{ER} = \frac{\rho_p}{\rho_f} \quad (4)$$

2.8.4. Thermogravimetric Analysis (TGA)

To determine the thermal stability of the inclusion complex, as well as to evaluate the effect of supercritical processing (impregnation or foaming) on the structural characteristics of the polymeric mixture. Thermogravimetric analysis (TGA) was used to determine the type of degradation and also to evaluate the thermal stability of the different films and foams developed in this work. This analysis was performed at 10 $^{\circ}\text{C}/\text{min}$, between 25 and 700 $^{\circ}\text{C}$, under nitrogen atmosphere, in an SDT 2960 DSC-TGA (TA Instruments, New Castle, DE, USA).

2.8.5. Differential Scanning Calorimetry (DSC)

The crystallization behavior of pure polymers, films, and foams of PLA/PBAT blends was performed using a DSC model 822e (Mettler Toledo, Columbus, OH, USA) differential scanning calorimeter (DSC). Samples (5–7 mg) were heated from -50 $^{\circ}\text{C}$ to 200 $^{\circ}\text{C}$ at a rate

of 10 °C/min in a nitrogen atmosphere [48]. The degree of crystallinity of the films and foams was calculated by the following Equation (5):

$$x_c(\%) = \frac{\Delta H_m - \Delta H_{cc}}{w \cdot \Delta H_{m0}} \times 100\% \quad (5)$$

where ΔH_m is melting enthalpy, ΔH_{cc} is the cold-crystallization enthalpy, w is the weight fraction of PLA in the blend, and ΔH_{m0} is the melting enthalpy in 100% crystalline PLA, which has a value of 93.6 J/g [49].

2.9. Statistical Analysis

An analysis of variance (ANOVA) and Fisher's test were applied to evaluate the mean differences (with a confidence interval of 95 %) of the results of the thermal properties (DSC and TGA), using the statistical program Statgraphics Plus 5.1 (StatPoint®, Inc., Warrenton, VA, USA).

3. Results and Discussions

3.1. Characterization of Inclusion Complex IC

It is known that the ability of the CD to form inclusion complexes is strongly influenced by the size, shape, hydrophobicity, and form of the host molecule [26]. In addition, there are thermodynamic interactions between the different components of the system (cyclodextrin, host, and solvent), as there must be a favorable energetic driving force that attracts the host to the CD. The inclusion complexes formed by β -cyclodextrin (β -CD) and caffeic acid (CA) used in this study were characterized by an entrapment efficiency of 25%, similar to that reported by Kalogeropoulos and co-workers [50], who used β -CD to encapsulate propolis extract containing caffeic acid among its constituents. Efficiency was measured for each constituent of the extract using an ethanol solution, where 19.4% efficiency was obtained. These results could be related to the fact that a pH equal to 5 in the ethanol-water solution causes the CA structure to be deprotonated in the carboxylic acid group in its COO^- form, which causes an increase in the polarity of the active ingredient [51,52]. On the other hand, the presence of ethanol can lead to a decrease in the polarity of the medium, which weakens the driving force for inclusion complex formation [53].

The molecular inclusion of CA in the hydrophobic cavity of the β -CD was evidenced by one-dimensional proton nuclear magnetic resonance ($^1\text{H-NMR}$), where the bands associated with the hydrogens belonging to the host and the guest were analyzed. Figure 2 shows the chemical structures of both compounds (CA and β -CD) and the partial $^1\text{H-NMR}$ of CA, β -CD, and IC in D_2O . The chemical shifts (δ) of the internal (H-3 and H-5) and external (H-1, H-2, H-4, and H-6) protons of the β -cyclodextrin and inclusion complex [54], CA (H-a, H-b, H-c, H-d, and H-e), and inclusion complex are shown in Table 2.

In Figure 2c, with respect to the CA and IC spectra, there is a shift mainly of the hydrogens associated with the aromatic ring of caffeic acid (H-b, H-c, and H-d), which could interact with the hydrophobic cavity of the cyclodextrin, while the most polar groups of the molecule, $-\text{COOH}$ and hydroxyl groups, would be outside the more hydrophilic cavity. This result has been reported by Chao and coworkers [51], who studied the molecular inclusion of hydroxypropyl cyclodextrin with caffeic acid. On the other hand, Figure 2d would confirm the interaction of the aromatic ring due to the displacement of the internal protons (H-3 and H-5) of the β -CD.

As shown in Table 2, the highest $\Delta\delta$ values can be observed at H-b, H-c, and H-d for CA/IC and H-5 with respect to β CD/IC. As reported by other authors [38,55–57], the difference in chemical shifts confirms the formation of the inclusion complex, as they

indicate significant variations between the cyclodextrin cavity and the guest (CA). These findings were corroborated by FTIR and TGA analysis.

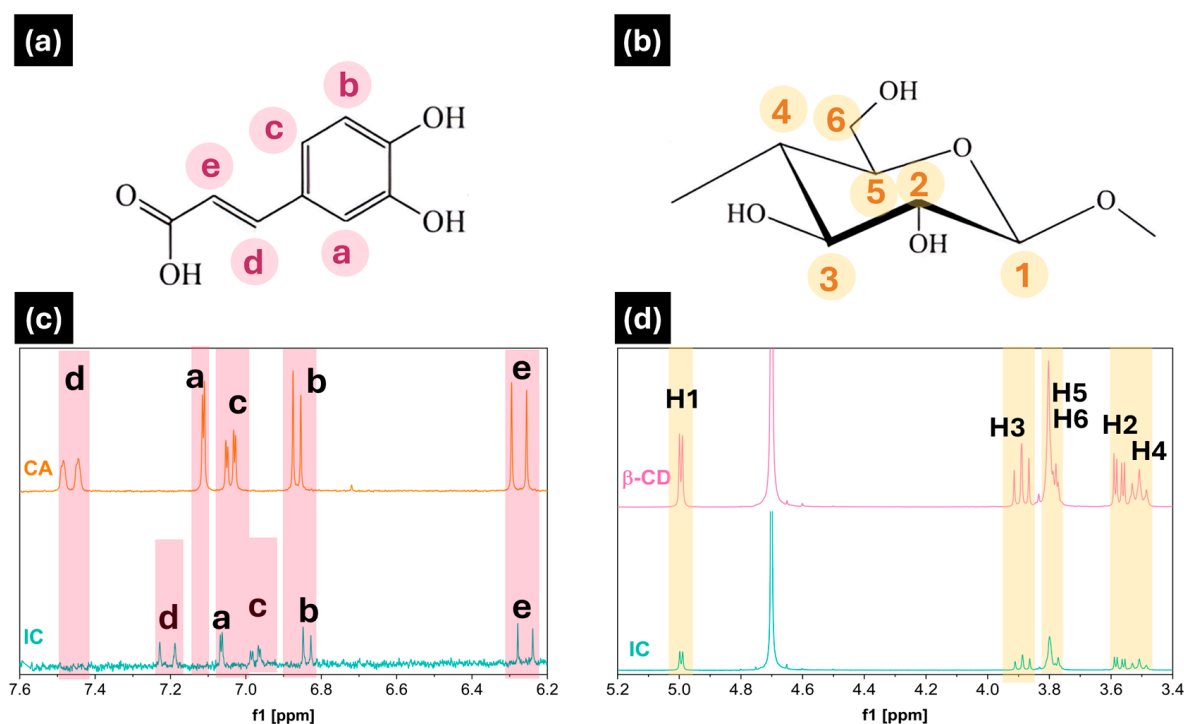


Figure 2. Structures of (a) caffeic acid and (b) β -Cyclodextrin. Partial $^1\text{H-NMR}$ partial spectra (c) caffeic acid (CA) and β -Cyclodextrin/caffeic acid (IC); (d) β -Cyclodextrin (β -CD) and β -Cyclodextrin/caffeic acid (IC), in D_2O .

Table 2. $^1\text{H-NMR}$ chemical shifts (δ , ppm) for CH protons of pure β -CD, pure CA, and their complexation-induced shifts ($\Delta\delta = \delta_{\text{complex}} - \delta_{\text{free}}$).

	δ_{Free}	δ_{Complex}	$\Delta\delta$
Ha	7.110	7.150	−0.04
Hb	6.875	6.848	0.027
Hc	7.033	6.940	0.093
Hd	7.445	7.220	0.225
He	6.295	6.367	−0.072
H-1	5.088	5.087	0.001
H-2	3.680	3.678	0.002
H-3	3.978	3.976	0.002
H-4	3.598	3.597	0.001
H-5	3.868	3.860	0.008
H-6	3.892	3.888	0.004

FTIR analyses allowed the identification of characteristic bands of the inclusion complex through vibrational and rotational motions of the molecular bonds. The formation of the IC inclusion complex involves the interaction of hydrogen bonds due to hydrophobic interactions of the internal cavity of the β -CD. The generated interactions are represented by the increase, decrease, or shift of certain characteristic frequencies in the spectrum. Figure 3 shows the spectra of CA, β -CD, and IC.

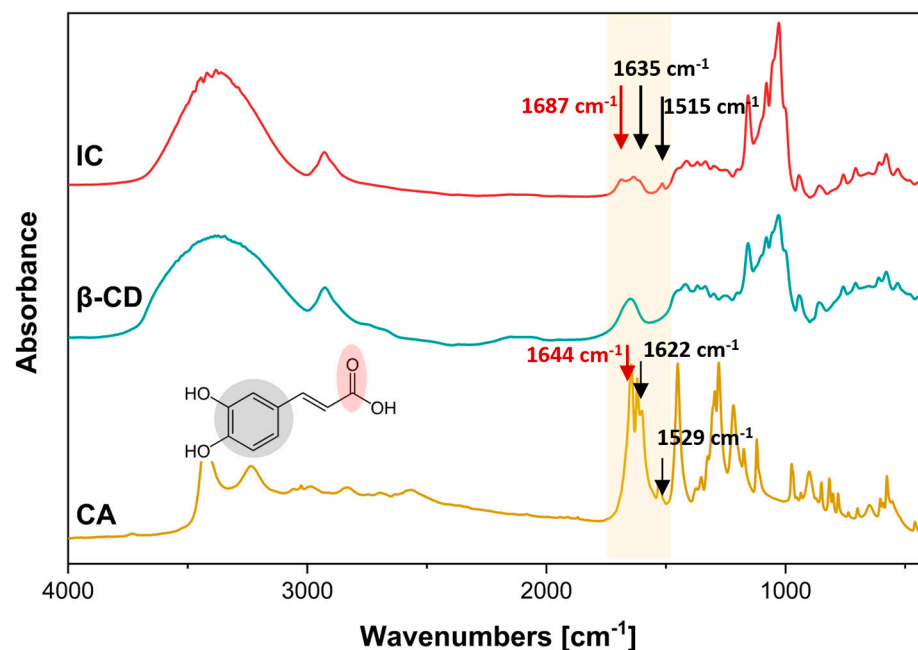


Figure 3. FTIR spectra of different compounds: CA; β -CD; IC.

In the spectrum of Figure 3, it is illustrated that β -CD exhibited a broad band at 3386 cm^{-1} , indicative of OH-stretching vibrations, and a band at 2926 cm^{-1} , associated with the C-C bond tension of the polysaccharide. Additionally, a band was observed at 1649 cm^{-1} . The band at 1251 cm^{-1} is attributed to the asymmetric stretching vibration of the glycosidic bond, while the intense absorption at 1029 cm^{-1} is due to the C-O-C stretching of the alcohol [58]. The latter is also evidenced by the band at 3386 cm^{-1} , which is related to the OH-stretching vibrations. In the case of CA, the OH groups of its aromatic ring can be observed at 3433 cm^{-1} [55]. The IC spectrum (Figure 4) shows a shift and decrease in the CA bands in the carbonyl groups (C=O) from 1644 cm^{-1} to 1687 cm^{-1} and in the aromatic moiety (C=C) at 1622 cm^{-1} to 1635 cm^{-1} and at 1515 cm^{-1} . Finally, these results allow us to suggest that the CA is within the hydrophobic cavity of the cyclodextrin [57].

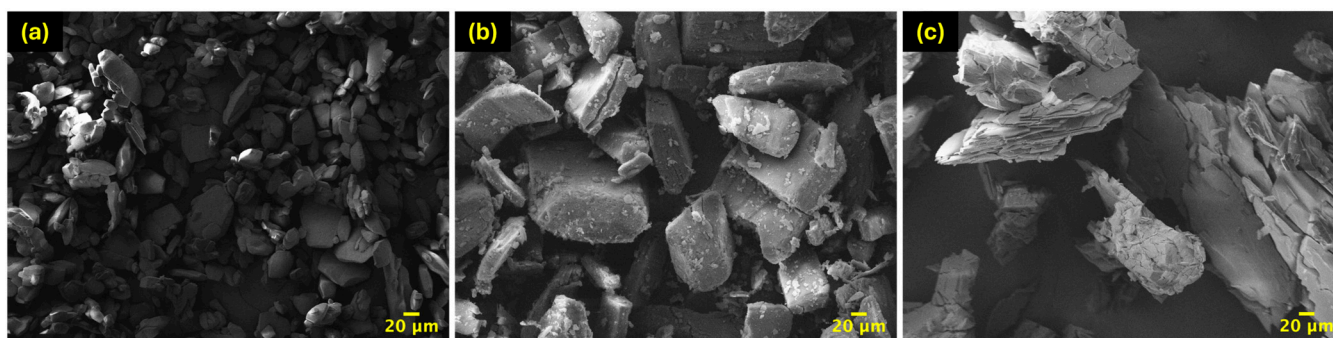


Figure 4. SEM micrographs of (a) β -CD; (b) IC at $500\times$ and (c) CA at $500\times$.

The morphological structure of β -CD, CA, and IC particles was characterized by SEM. As shown in Figure 4, the surface of the IC is rough and exhibits cracks in accordance with that inclusion complex synthesized by Zhang and coworkers [59]. However, the structural features of the host cyclodextrin were preserved when the IC. In contrast, both β -CD and CA particles displayed a smooth surface with square-shaped, consistent with micrographs reported in the literature [60,61].

Finally, with regard to thermal stability, Figure 5 presents the thermograms (TG and DTG) of IC and the pure compounds (CA and β -CD). The β -CD exhibited a mass loss at two distinct temperatures, below 100 °C, attributable to water loss, and subsequently at around 330 °C, corresponding to the thermal decomposition of the β -CD [62]. CA, on the other hand, exhibited stability above 150 °C and underwent a two-step thermal decomposition process. The initial step, characterized by a weight loss of 20%, involved the melting and degradation of CA at 228 °C. The subsequent step, attributed to acid decarboxylation, occurred at 335 °C and resulted in a weight loss of approximately 60% [23,63].

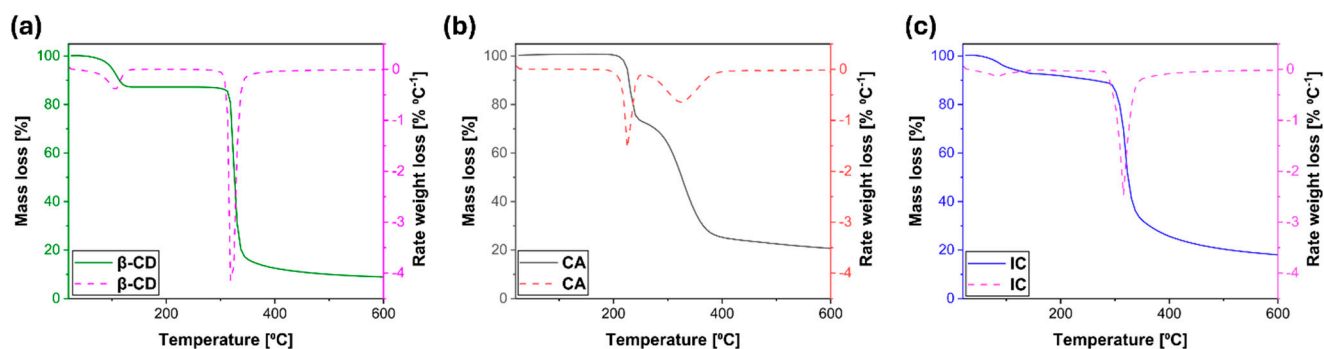


Figure 5. TG and DTG thermograms of (a) β -cyclodextrin (β -CD), (b) caffeic acid (CA), and (c) inclusion complex (IC) samples.

On the other hand, in Figure 5c, the IC shows a first region corresponding to a slight loss of mass of 6% below 100 °C, which is attributed to the presence of water [64]. In addition, a second region around 315 °C shows the highest mass loss. As for the endothermic peaks (150 and 228 °C) associated with the decomposition of CA, none are observed. This would indicate that the formation of IC protects CA from thermal degradation.

3.2. Quantification of Caffeic Acid (CA) in Impregnated Films and Foams

With regard to the sensitivity of the method, a detection and quantification limit equivalent to 3.32 $\mu\text{g/L}$ and 10.05 $\mu\text{g/L}$ was obtained, respectively. The lowest concentration value of caffeic acid quantified was 12.6 $\mu\text{g/L}$. The IC impregnation process in PLA and PLA/PBAT blends contemplated the best operating conditions for samples incorporating pure CA, which were obtained from a previous work [41] that impregnated the same polymeric matrices. Based on this, Figure 6 presents the results obtained, considering a constant temperature of 40 °C, with a CO_2 density of 718 (12 MPa) and 780 kg/m^3 (15 MPa) [65], as well as a cosolvent concentration of 0 and 5% *w/w* ethanol.

The incorporation of ethanol as a cosolvent (5% *w/w*) into the polymer matrix resulted in an augmentation of CA, both for pure CA and IC impregnations. The addition of small amounts of scCO_2 -soluble polar cosolvent (ethanol) has been demonstrated to enhance the plasticizing effect of CO_2 on the polymer. Furthermore, the incorporation of ethanol into the supercritical phase enhances the solubility of the active compound by improving the polarity of the high-pressure phase and, consequently, its solvating capacity. This was also reported by Bitencourt et al. [66], who analyzed the solubility of caffeic acid in scCO_2 at different pressures and temperatures and obtained a significant increase when ethanol was used as a cosolvent, since the presence of a polar solvent induces specific interactions, such as hydrogen bonding interactions, between the solute and the solvent.

With respect to the PLA(4)/PBAT(84) blend, a different trend was obtained compared to the other polymeric matrices when the impregnation was performed in the cosolvent presence. This discrepancy can be attributed to CO_2 solubility in PBAT, which is 8.5 g $\text{CO}_2/100$ g polymer (15 MPa and 40 °C), as compared to that of PLA, which is 22.6 g $\text{CO}_2/100$ g polymer (15 MPa and 40 °C) [67]. Additionally, the presence of CaCO_3 in the

blend may also influence the impregnation of the active compound. The efficiency of the supercritical impregnation process depends largely on the interactions in a ternary system composed of the active agent, the polymeric matrix, and CO₂.

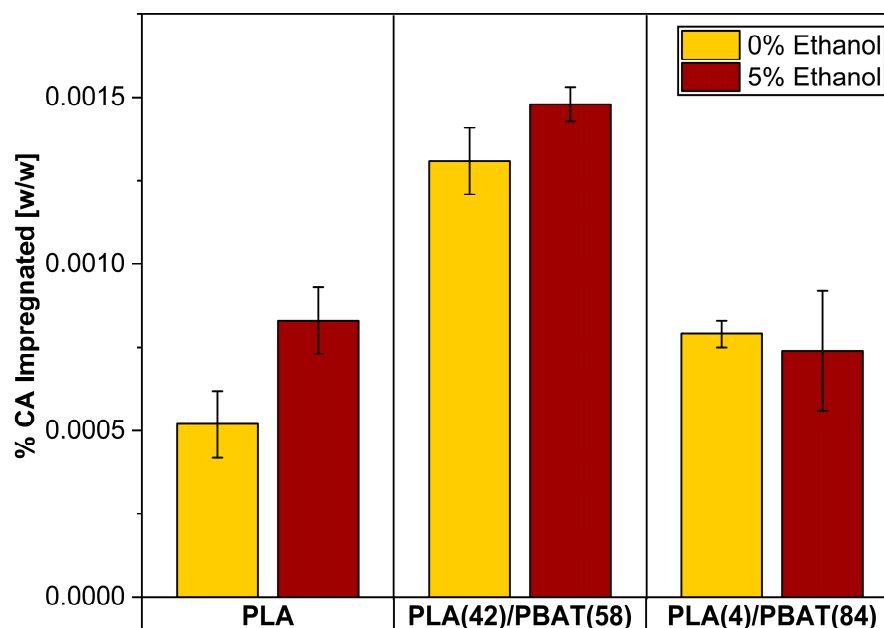


Figure 6. Amount of caffeic acid (expressed as % *w/w*), incorporated in PLA, PLA(42)/PBAT(58) and PLA(4)/PBAT(84) films, by supercritical impregnation of the inclusion complex.

Regarding the low impregnation rates obtained when using IC, it can be explained by the low solubility of the active compound in scCO₂ due to the high polarity of CA and β-CD (due to hydroxyl groups oriented in the outer layer of the molecule), hindering the transport of the active towards the polymeric matrix, which leads to low impregnation yields. The low affinity of these compounds in scCO₂ could explain the low amount of impregnated CA. When comparing these results with those obtained by, which used PLA, PLA(42)/PBAT(58), and PLA(4)/PBAT(84) with and without ethanol under similar operating conditions, with an experimental matrix that only contemplated the use of caffeic acid without cyclodextrins, obtained an impregnation rate of 0.0055% (mg CA/mg polymer) in the PLA(42)/PBAT(58) polymer at a pressure of 12 MPa with a depressurization rate of 1 MPa/min and with the use of ethanol as cosolvent at 5%. Cejudo and coworkers impregnated caffeic acid in polyethylene terephthalate films with polypropylene (PET/PP) using pressures between 10 and 40 MPa and obtained a maximum impregnation rate of 0.006%, which was due to the low solubility of the active in scCO₂ and the limited affinity of caffeic acid in the films [68]. This accounts for the fact that supercritical impregnation is highly dependent on the interaction and equilibrium of the ternary system, i.e., polymer matrix/active agent/scCO₂. This includes the effect of pressure, temperature, and/or structural change of the polymer on the solubility, diffusivity, and partition coefficient in the system [69,70].

Finally, the effect of the supercritical foaming process at 15 and 25 MPa on the impregnated films was evaluated at the conditions of higher incorporation of caffeic acid with and without IC, which is presented in Table 3.

Table 3 shows a decrease in the amount of CA in all polymers after foaming. This is due to the fact that the impregnated foams are again exposed to scCO₂, so that the inclusion complex is resolubilized by the fluid, dragging it at the moment of generating the depressurization of the system [71]. As for the differences in the amounts of compound loaded in the polymer, it can be attributed to the pressures of 15 and 25 MPa used in

the foaming process, which causes the density of scCO₂ to vary at 262 and 471 g/mL, respectively. As expected, the higher the pressure, the higher the density of scCO₂ and thus the ability of both compounds to dissolve in the medium [72,73]. Although this variable affects the compounds equally, CA still has a higher affinity for the medium compared to IC, because it has a non-polar end, so it solubilizes better in the medium. On the other hand, when depressurizing the system, less compound is lost when using IC. This occurs because the CA is inside the cavity of the β -CD, which hinders the interaction of the molecule with the medium. In addition, the cyclodextrin presents in its outer layer a large amount of OH groups, a phenomenon that can be observed in the FTIR spectrum of IC. This polarity difference causes a low affinity between IC and scCO₂, reducing the amount of compound entrained during depressurization [66].

Table 3. Variation in impregnated caffeic acid in PLA films and PLA/PBAT blends upon foaming.

Sample	Type	Pressure [MPa]	% CA [<i>w/w</i>]
PLA/IC	Film	-	0.00096 ± 0.0001
PLA/15/IC	Foam	15	0.00085 ± 0.0001
PLA/25/IC	Foam	25	0.00085 ± 0.0001
PLA(42)/PBAT(58)/IC	Film	-	0.0015 ± 0.0001
PLA(42)/PBAT(58)/15/IC	Foam	15	0.0013 ± 0.0001
PLA(42)/PBAT(58)/25/IC	Foam	25	0.0014 ± 0.0002
PLA(4)/PBAT(84)/IC	Film	-	0.00082 ± 0.0001
PLA(4)/PBAT(84)/15/IC	Foam	15	0.00082 ± 0.0001
PLA(4)/PBAT(84)/25/IC	Foam	25	0.00073 ± 0.0001

Films results are shown in bold type.

3.3. Characterization of the Materials Obtained (Films and Foams)

3.3.1. ATR-FTIR Analysis

The structural analysis of the films and foams (denoted with the subscript F) developed was conducted using Fourier transform infrared spectroscopy—attenuated total reflectance (FTIR-ATR) analyses. These analyses were performed to ascertain the characteristic functional groups of each polymer. These groups were identified by distinct bands that indicate vibrations and stretching associated with their chemical bonds.

The characteristic bands of PLA, such as carbonyl groups (C=O) at 1747 cm⁻¹, stretching of methyl groups (CH₃) at 1453 and 1380 cm⁻¹ [74,75], and two signals associated with asymmetric C-O-C and C-O vibrations at 1180 and 1079 cm⁻¹ [76], respectively, could be observed in all samples shown in Figure 7A. In addition, the bands observed at 867 cm⁻¹ and 754 cm⁻¹ are attributed to C-C bond stretching, a characteristic feature of the amorphous and crystalline phases of PLA [39,77].

In contrast, a distinguishing feature of PLA relative to PBAT is the presence of phenyl rings, as evidenced by the spectra in Figure 7B,C at a wavenumber of 1015 cm⁻¹ [48,54]. Furthermore, the analysis revealed the presence of signals from the C=O stretching of the carbonyl and ester groups in both mixtures at 1712 cm⁻¹, a band at 1267 cm⁻¹ belonging to the stretching of the C-O ester groups, and a strong signal at 727 cm⁻¹ corresponding to the stretching of the CH₂ groups [78].

While PLA (Figure 7A(a)) films exhibited clear variations at 1210 cm⁻¹ due to the vibration of the C-O-C group resulting from the asymmetric oscillation of CH₃, additional peaks emerged at 956 and 920 cm⁻¹. These peaks corresponded to relative changes in the PLA amorphous fraction (decreased due to the presence of IC) and the α -crystalline phase, respectively.

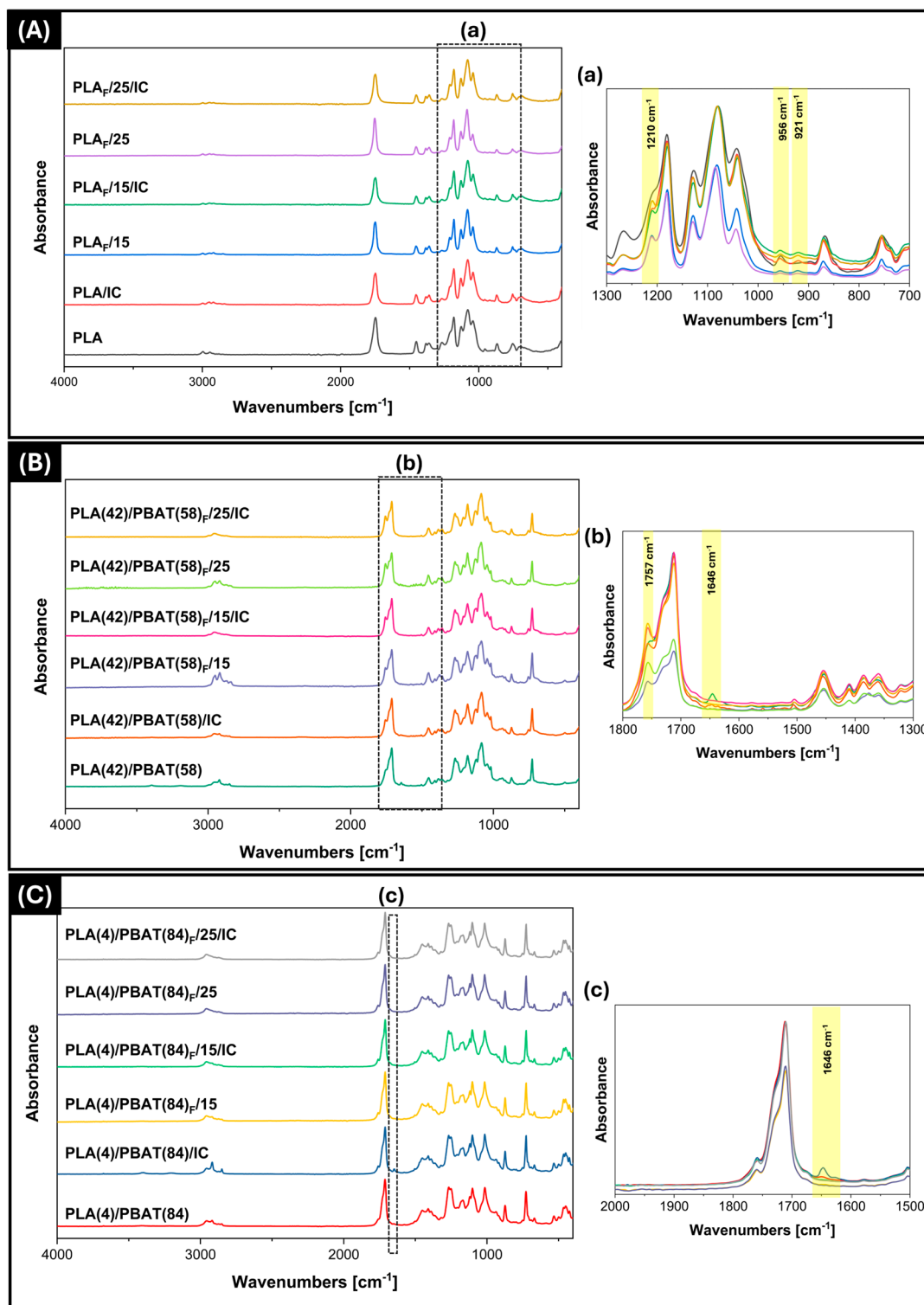


Figure 7. FTIR spectra of films and foams (F as subindex) of: (A) PLA, (B) PLA(42)/PBAT(58), (C) PLA(4)/PBAT(84), with and without the inclusion complex. (a) PLA spectrum in the region 1300–700 cm⁻¹, (b) PLA(42)/PBAT(58) spectrum in the region 1800–1300 cm⁻¹, (c) PLA(4)/PBAT(84) spectrum in the region 2000–1500 cm⁻¹.

The increase in bands may be due to the effect of IC on PLA crystallization as demonstrated in the DSC tests below, as well as the rearrangement of amorphous to crystalline phases, which may be in individual regions or throughout the polymer. Meaurio and coworker [79] evaluated the effect of PLLA crystallinity by Fourier infrared spectroscopy,

showing that as the crystallinity of the polymers increases, the intensity of the bands also increases.

Finally, changes in the band at 1646 cm^{-1} were observed in the films with and without IC of PLA(42)/PBAT(58) and PLA(4)/PBAT(84) (Figure 7B(b),C(c)). These changes may be related to the CO_2 impregnation process, as CO_2 produces a swelling effect that generates polymer chain mobility and subsequently reduces IR penetration. This may indicate that the swelling effect of the polymer matrix is partially irreversible and/or the polymer chain order is modified after depressurizing the system [80].

3.3.2. Thermogravimetric Analysis (TGA)

To assess the effect of the incorporation of the inclusion complex, the supercritical impregnation process, and the pressure variation during foaming on the thermal stability of PLA films and PLA/PBAT blends, thermogravimetric analyses were performed. The values obtained from the thermograms are shown below in Table 4, in bold italics, the results for pure and impregnated films are shown, while the foams are shown with a letter F as a subindex.

Table 4. Onset of degradation (T_{onset}) and maximum degradation temperatures (T_{max}) of films and foams with and without IC.

Sample	Pressure [MPa]	Initial Degradation Temperature [$^{\circ}\text{C}$]			Maximum Degradation Temperature [$^{\circ}\text{C}$]		
		1	2	3	1	2	3
PLA		<i>344.9 ± 0.9^{a,b,c}</i>	<i>N.D.</i>	<i>N.D.</i>	<i>361.8 ± 0.9^{a,b}</i>	<i>N.D.</i>	<i>N.D.</i>
PLA/IC		<i>348.1 ± 1.2^a</i>	<i>N.D.</i>	<i>N.D.</i>	<i>363.2 ± 0.7^a</i>	<i>N.D.</i>	<i>N.D.</i>
PLA _F	15	<i>341.8 ± 2.3^{a,b,c,d}</i>	<i>N.D.</i>	<i>N.D.</i>	<i>360.4 ± 1.3^{a,b}</i>	<i>N.D.</i>	<i>N.D.</i>
PLA _F /IC		<i>348.2 ± 0.7^a</i>	<i>N.D.</i>	<i>N.D.</i>	<i>362.9 ± 0.5^a</i>	<i>N.D.</i>	<i>N.D.</i>
PLA _F	25	<i>346.9 ± 1.7^{a,b}</i>	<i>N.D.</i>	<i>N.D.</i>	<i>362.6 ± 0.4^a</i>	<i>N.D.</i>	<i>N.D.</i>
PLA _F /IC		<i>347.5 ± 0.5^{a,b}</i>	<i>N.D.</i>	<i>N.D.</i>	<i>362.9 ± 0.1^a</i>	<i>N.D.</i>	<i>N.D.</i>
PLA(42)/PBAT(58)		<i>337.3 ± 3.3^{c,d}</i>	<i>388.7 ± 1.1^d</i>	<i>N.D.</i>	<i>358.1 ± 0.9^{a,b}</i>	<i>400.1 ± 2.9^j</i>	<i>N.D.</i>
PLA(42)/PBAT(58)/IC		<i>340.2 ± 0.1^{b,c,d}</i>	<i>392.2 ± 0.2^a</i>	<i>N.D.</i>	<i>357.7 ± 1.2^{a,b}</i>	<i>403.3 ± 0.1^f</i>	<i>N.D.</i>
PLA(42)/PBAT(58) _F	15	<i>337.7 ± 1.2^{c,d}</i>	<i>387.2 ± 1.9^e</i>	<i>N.D.</i>	<i>357.1 ± 0.2^{a,b}</i>	<i>399.2 ± 0.2^k</i>	<i>N.D.</i>
PLA(42)/PBAT(58) _F /IC		<i>336.3 ± 0.1^d</i>	<i>391.1 ± 2.1^c</i>	<i>N.D.</i>	<i>355.5 ± 3.1^b</i>	<i>402.6 ± 0.3^h</i>	<i>N.D.</i>
PLA(42)/PBAT(58) _F	25	<i>335.3 ± 2.6^d</i>	<i>383.9 ± 5.5^f</i>	<i>N.D.</i>	<i>355.6 ± 2.3^{a,b}</i>	<i>400.8 ± 1.9^l</i>	<i>N.D.</i>
PLA(42)/PBAT(58) _F /IC		<i>338.2 ± 1.3^{c,d}</i>	<i>391.1 ± 0.1^b</i>	<i>N.D.</i>	<i>356.9 ± 3.6^{a,b}</i>	<i>400.2 ± 3.5ⁱ</i>	<i>N.D.</i>
PLA(4)/PBAT(84)		<i>314.5 ± 0.6^{e,f}</i>	<i>378.6 ± 0.7^k</i>	<i>555.5 ± 5.5^a</i>	<i>328.9 ± 0.9^c</i>	<i>403.5 ± 0.3^d</i>	<i>586.5 ± 0.5^a</i>
PLA(4)/PBAT(84)/IC		<i>314.6 ± 0.3^{e,f}</i>	<i>378.9 ± 0.1^j</i>	<i>563.3 ± 9.3^a</i>	<i>328.1 ± 0.2^{c,d}</i>	<i>404.6 ± 0.5^a</i>	<i>597.2 ± 6.8^a</i>
PLA(4)/PBAT(84) _F	15	<i>310.2 ± 0.5^f</i>	<i>378.1 ± 3.9^l</i>	<i>552.9 ± 11.7^a</i>	<i>322.0 ± 2.1^d</i>	<i>402.8 ± 1.7^g</i>	<i>592.7 ± 13.3^a</i>
PLA(4)/PBAT(84) _F /IC		<i>310.6 ± 1.5^f</i>	<i>379.2 ± 0.1^h</i>	<i>559.1 ± 4.9^a</i>	<i>327.2 ± 1.2^{c,d}</i>	<i>403.9 ± 0.1^b</i>	<i>592.2 ± 3.0^a</i>
PLA(4)/PBAT(84) _F	25	<i>320.3 ± 5.2^e</i>	<i>384.7 ± 5.3^g</i>	<i>559.6 ± 7.1^a</i>	<i>326.6 ± 3.5^{c,d}</i>	<i>403.3 ± 1.0^e</i>	<i>597.8 ± 6.3^a</i>
PLA(4)/PBAT(84) _F /IC		<i>315.3 ± 1.8^{e,f}</i>	<i>379.1 ± 0.1ⁱ</i>	<i>562.2 ± 6.9^a</i>	<i>329.3 ± 1.3^c</i>	<i>403.7 ± 0.4^c</i>	<i>590.7 ± 1.4^a</i>

N.D. not detected. Films results are shown in bold type. Lowercase letters a–l indicate significant differences between the values of each thermal parameter.

Regarding the pure materials (prior to the supercritical impregnation process), PLA presents a one-stage thermal degradation, with an initial degradation temperature (T_{onset}) equal to $344\text{ }^{\circ}\text{C}$. On the other hand, the PLA(42)/PBAT(58) mixture presented a 2-stage thermal degradation, the first ($337\text{ }^{\circ}\text{C}$) corresponds to the presence of PLA, and the second to PBAT ($388\text{ }^{\circ}\text{C}$), which has a higher thermal stability with respect to PLA because it has a benzene ring in its structure that allows it to withstand higher temperatures.

The PLA(4)/PBAT(84) mixture exhibited a third degradation stage at $586\text{ }^{\circ}\text{C}$, indicative of the presence of inorganic matter. According to previous research by other authors, this corresponds to the decomposition of calcium carbonate (CaCO_3) into carbon dioxide and calcium oxide (CaO) [81]. The observed reduction in the thermal stability of PLA is attributable to the catalytic effect of CaCO_3 in depolymerizing the ester bond, a process that is facilitated by the presence of a metal ion (Ca^{2+}) and the subsequent formation of free radicals and reactive terminal groups during the decomposition of polyesters [82,83].

On the other hand, in the samples impregnated with the inclusion complex, changes were only observed in the PLA(42)/PBAT(58)/IC samples, this would agree with the results in the quantification analyses, since this sample presented a greater amount of impregnated active agent. The increase in the initial degradation temperature of PBAT could be related to its chemical structure, since it presents two carbonyl groups, with which the inclusion complex could be interacting.

In the case of foamed samples, it is important to clarify that the foams without active compound were only exposed once to scCO_2 , while the active ones were subjected to supercritical impregnation and then foamed. With respect to the active and pure samples, no statistically significant differences in their thermal stability were observed, suggesting that supercritical reprocessing of the material does not contribute to changes in the different materials.

3.3.3. Differential Scanning Calorimetry (DSC)

Differential scanning calorimetry (DSC) was utilized to ascertain the impact of the samples with the most substantial IC incorporation during the impregnation process on their transition temperatures. Figure 8 and Table 5 present the results obtained for PLA and PLA/PBAT blend impregnated films, as well as films that were not exposed to CO_2 and IC, in order to discern potential structural alterations induced by the impregnation of the active compound.

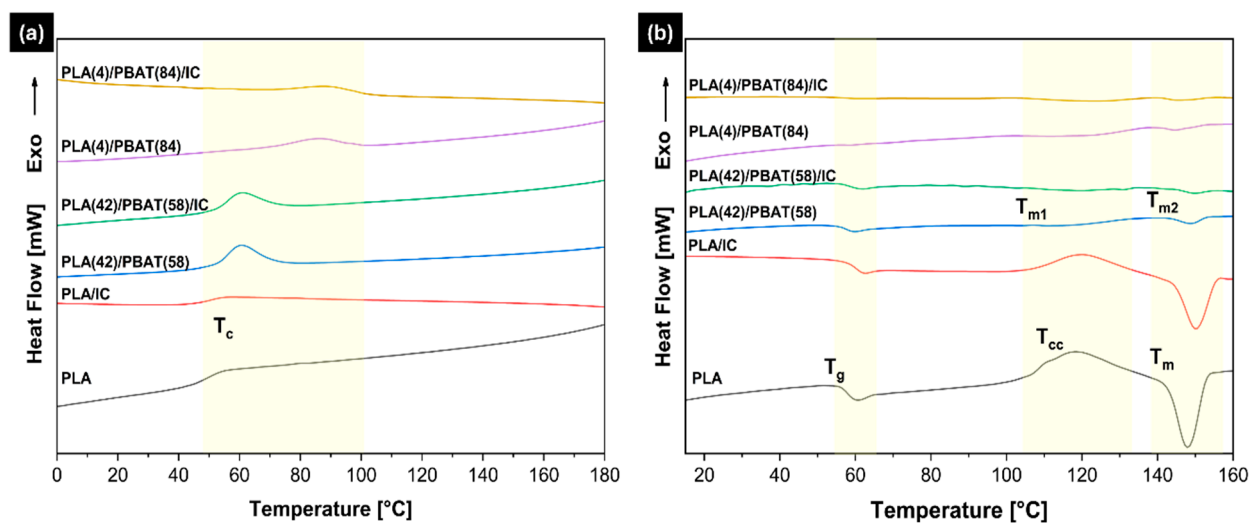


Figure 8. (a) Cooling and (b) 2nd heating curves in the DSC thermograms of films of PLA, PLA(42)/PBAT(58), PLA(4)/PBAT(84), with and without the inclusion complex.

Table 5. Thermal parameters of control and impregnated films with and without IC.

Sample	T_g PBAT [°C]	T_g PLA [°C]	T_m PBAT [°C]	H_m PBAT [J/g]	T_m PLA [°C]	H_m PLA [J/g]	X_c PLA [%]
PLA	N.D.	58.1 ± 0.2^a	N.D.	N.D.	148.2 ± 0.2^b	29.2 ± 0.4^a	4.1 ± 0.2^b
PLA(42)/PBAT(58)	-31.3 ± 0.1^c	57.4 ± 1.1^a	115.1 ± 0.1^d	7.1 ± 0.4^a	148.9 ± 0.2^b	2.2 ± 0.1^b	5.7 ± 0.2^b
PLA(4)/PBAT(84)	-32.0 ± 2.6^d	56.6 ± 0.3^a	123.4 ± 0.1^b	4.4 ± 0.2^c	145.8 ± 0.1^c	1.5 ± 0.1^b	39.0 ± 2.6^a
PLA/IC	N.D.	58.5 ± 0.3^a	N.D.	N.D.	$149.6 \pm 0.8^{a,b}$	28.7 ± 0.5^a	4.0 ± 0.2^b
PLA(42)/PBAT(58)/IC	-29.5 ± 0.3^b	56.9 ± 0.2^a	120.2 ± 0.7^c	3.7 ± 0.4^d	151.1 ± 0.4^a	1.3 ± 0.1^b	3.2 ± 0.1^b
PLA(4)/PBAT(84)/IC	-27.9 ± 0.1^a	56.9 ± 0.7^a	123.8 ± 0.6^a	4.3 ± 0.1^b	145.6 ± 0.1^c	1.4 ± 0.1^b	37.1 ± 2.3^a

Lowercase letters a–d indicate significant differences between the values of each thermal parameter. N.D.: Not detected.

As demonstrated in Table 5, the PLA/PBAT blends exhibited two glass transition regions, at temperatures of -31 °C for PBAT and 56 °C corresponding to the melting

point of PLA. This observation indicates that the blends are immiscible and exhibit a two-phase structure [42], a phenomenon analogous to that reported by Chiu and coworkers [84]. In their study, PLA/PBAT blends with varying proportions were obtained by means of injection molding, with glass transition temperatures for PBAT ranging from -35 to -30 °C and for PLA from 57 to 61 °C. In comparison between the PLA(42)/PBAT(58) and PLA(4)/PBAT(84) mixture, the latter presented a statistically significant increase in T_m of PBAT and X_c of PLA. The rise in X_c PLA can be ascribed to the synergistic impact of two elements: firstly, the elevated percentage of PBAT (84%) within the mixture, and secondly, the presence of calcium carbonate (CaCO_3), which constitutes the remaining 12% of the inert matter stipulated for this blend. The concomitant presence of PBAT and CaCO_3 has been demonstrated to enhance the crystallization behavior of PLA, as evidenced by studies indicating that rigid CaCO_3 particles function as nucleating agents, thereby contributing to enhanced crystallinity [83,85,86].

The thermograms presented in Figure 8 reveal that pure PLA, with and without IC, exhibited an exothermic peak of cold crystallization T_{cc} around 120 °C during the second heating (Figure 8b). This phenomenon is attributed to the recrystallization of PLA. This confirms what was reported by other authors about the slow crystallization rate of PLA, since it does not occur in a single step during cooling, which generates a partial realignment of its molecular chains during the second heating.

On the other hand, the thermal behavior of the PLA/PBAT blend films was different. During the cooling step, the DSC thermograms of both blends (Figure 8a) showed an exothermic signal, mainly related to the induction of PLA crystallization by the presence of PBAT. T_c values ranged between 60 and 85 °C for the PLA(42)/PBAT(58) and PLA(4)/PBAT(84) blends, respectively. The increase in temperature and the decrease in the intensity of the exothermic peak for the mixture presenting a higher proportion of PBAT could be due to the influence of CaCO_3 which, acting as a nucleating agent, also contributes to accelerating the crystallization rate. Therefore, in both PLA/PBAT blends, recrystallization of PLA molecular chains did not occur during the second heating, leading to the disappearance of the T_{cc} peak [87].

With respect to IC incorporation, an increase in the melting temperature of PLA and PBAT was observed, which is related to the increase in Van der Waals forces. The increase in Van der Waals forces can be attributed to the interaction of the polymer chains with IC. On the other hand, the PLA(42)/PBAT(58) blend showed a decrease in the enthalpy of fusion for the PBAT fraction, which is attributed to the decrease in the crystalline zones [88]. However, no statistically significant changes were observed for X_c , which could be related to the distribution of inclusion complexes in the polymer matrix.

Taking into account that crystallization affects cell growth, the relationship between foam cell morphology and the crystals it contains was evaluated. For the purpose of analysis, the initial heating of the DSC thermograms was examined to illustrate the alterations induced by the incorporation of PBAT into the mixtures and the subsequent processing with sCO_2 . The results of T_m , H_m , and X_c of PLA for foams with and without IC are presented in Table 6.

Table 6 shows that both the control samples and the samples with IC presented differences mainly in the enthalpy of fusion (ΔH_m) and the degree of crystallinity ($\%X_c$). According to the literature, this phenomenon is attributed to the crystallization that occurs during the foaming process [49]. The absorption of additional CO_2 , which is a consequence of heightened pressure, leads to substantial swelling of the polymer matrix. This, in turn, results in a plasticizer effect that facilitates the reorientation of polymer chains at a reduced free energy [89]. While the foams previously impregnated with IC presented a statistically significant increase in X_c , only in PLA(42)/PBAT(58) at 15 MPa, which presented a higher

amount of impregnated active. This could be related to the heterogeneous nucleation effect caused by the incorporation of the inclusion complex into the polymeric matrix, as reported by other authors [88,90].

Table 6. Thermal parameters of control and impregnated foams with and without IC.

Sample	Pressure [MPa]	T _m PLA [°C]	ΔH _m [J/g] PLA	%X _c PLA
PLA _F	15	153.5 ± 0.6 ^{a,b}	46.1 ± 4.3 ^a	49.2 ± 4.6 ^{b,c}
PLA(42)/PBAT(58) _F		152.5 ± 0.1 ^{a,b,c}	9.9 ± 0.7 ^d	25.1 ± 1.8 ^g
PLA(4)/PBAT(84) _F		150.9 ± 0.2 ^{b,c,d}	2.0 ± 0.1 ^e	52.1 ± 2.3 ^{a,b}
PLA _F	25	148.9 ± 0.4 ^{d,e,f}	33.0 ± 0.4 ^b	35.2 ± 0.4 ^{e,f}
PLA(42)/PBAT(58) _F		147.2 ± 0.5 ^{e,f}	15.2 ± 2.3 ^c	38.7 ± 5.9 ^{d,e}
PLA(4)/PBAT(84) _F		147.3 ± 0.2 ^{e,f}	1.0 ± 0.1 ^e	27.8 ± 2.6 ^{f,g}
PLA _F /IC	15	155.1 ± 0.9 ^a	43.5 ± 1.2 ^a	46.5 ± 1.3 ^{b,c,d}
PLA(42)/PBAT(58) _F /IC		153.4 ± 3.1 ^{a,b}	17.3 ± 2.3 ^c	43.9 ± 5.8 ^{c,d}
PLA(4)/PBAT(84) _F /IC		150.8 ± 1.1 ^{b,c,d}	2.2 ± 0.1 ^e	59.8 ± 3.4 ^a
PLA _F /IC	25	146.4 ± 1.3 ^f	32.4 ± 2.7 ^b	34.6 ± 6.4 ^{e,f}
PLA(42)/PBAT(58) _F /IC		147.2 ± 0.1 ^{e,f}	15.6 ± 0.1 ^c	39.6 ± 0.3 ^{d,e}
PLA(4)/PBAT(84) _F /IC		149.8 ± 3.3 ^{c,d,e}	1.1 ± 0.1 ^e	28.0 ± 1.5 ^{f,g}

Lowercase letters a–g indicate significant differences between the values of each thermal parameter.

3.4. Scanning Electron Microscopy (SEM)

Given that the morphology of foams is characterized by size (d), shape, cell density (NC), expansion coefficient (ER), and bulk density (ρ_f), the different foam samples obtained were analyzed by scanning electron microscopy (SEM). The results of this analysis are presented in Table 7.

Table 7. Cell diameter (d), foam density (ρ_f), cell density (NC), and expansion rate (ER).

Sample	Pressure [MPa]	d [μm]	ρ _f [kg/m ³]	NC [×10 ¹¹ Cell/cm ³]	ER
PLA	15	41.1 ± 8.4	104.7 ± 4.8	1.3	9.1
PLA(42)/PBAT(58)		52.0 ± 11.6	269.6 ± 1.5	0.5	3.3
PLA(4)/PBAT(84)		72.9 ± 19.9	203.6 ± 8.7	0.2	5.0
PLA	25	20.3 ± 4.1	197.5 ± 10.6	9.5	4.8
PLA(42)/PBAT(58)		32.7 ± 6.4	140.1 ± 15.6	2.5	6.4
PLA(4)/PBAT(84)		12.2 ± 2.9	295.5 ± 46.7	39.0	3.4
PLA/IC	15	26.7 ± 7.9	319.5 ± 9.8	3.6	3.3
PLA(42)/PBAT(58)/IC		43.7 ± 7.2	380.5 ± 38.2	0.7	3.3
PLA(4)/PBAT(84)/IC		23.9 ± 3.3	273.0 ± 37.4	5.2	2.6
PLA/IC	25	18.1 ± 5.9	181.1 ± 14.5	14.0	5.7
PLA(42)/PBAT(58)/IC		31.1 ± 6.3	152.4 ± 4.2	2.8	3.5
PLA(4)/PBAT(84)/IC		4.5 ± 1.4	335.9 ± 21.4	689.8	6.6

From Table 7, an increase in cell density can be observed, due to the presence of PBAT causing a heterogeneous nucleation effect. Figure 9 show a decrease in pore size is observed with increasing system pressure, and at the same time, the increase in CO₂ density (262.03–471.26 kg/m³) [65], which leads to a higher dissolution of the polymer in the supercritical phase, as well as a smaller cell size [91]. The influence of amorphous and crystalline structures on the formation of PLA foams is a subject of considerable interest. The presence of PBAT has been shown to modify the cell size, density, and expansion coefficient of PLA/PBAT-based foams, thereby influencing their crystalline behavior, as evidenced by DSC analysis. Results, like those obtained by Milovanovic et al. [92], who

obtained PLA foams with CO₂ densities from 273 kg/m³ to 630 kg/m³, with similar pore size behavior.

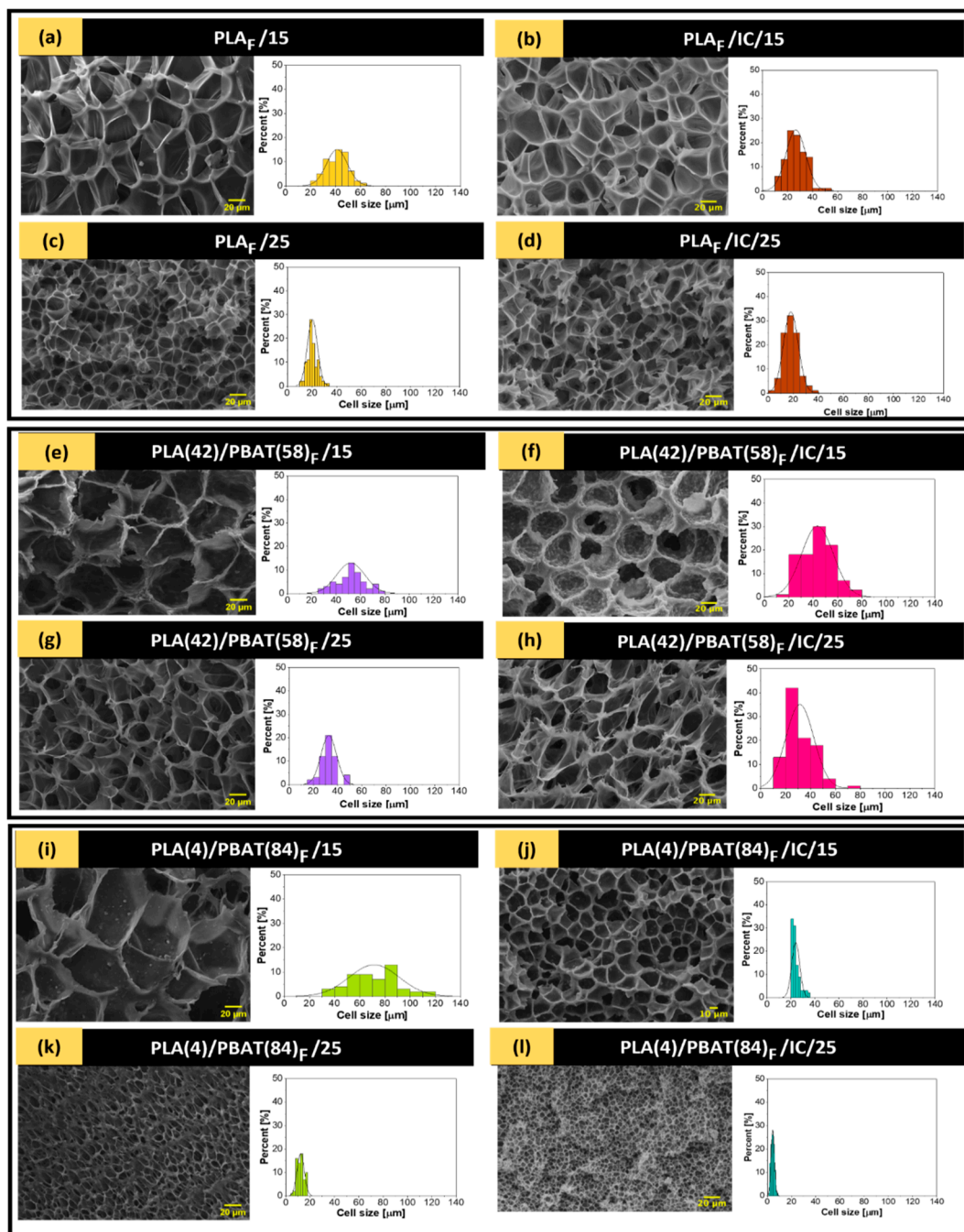


Figure 9. Left side: SEM micrographs of the cross section of 500× cold fractured samples of IC impregnated polymers (a) PLA_F/15, (b) PLA_F/IC/15, (c) PLA_F/25, (d) PLA_F/IC/25, (e) PLA (42)/PBAT(58)_F/15, (f) PLA (42)/PBAT(58)_F/IC/15, (g) PLA (42)/PBAT(58)_F/25, (h) PLA (42)/PBAT(58)_F/IC/25, (i) PLA(4)/PBAT(84)_F/15, (j) PLA(4)/PBAT(84)_F/IC/15, (k) PLA(4)/PBAT(84)_F/25, (l) PLA(4)/PBAT(84)_F/IC/25.

On the other hand, impregnation with IC in the polymers followed the trend of variation in cell diameter and density with increasing pressure, except for the PLA/IC polymer (Figure 9b,d), where at 25 MPa a larger cell diameter and a lower cell density were obtained compared to that formed at 15 MPa. This may be due to the decrease in the crystallinity of this polymer at 25 MPa, where a less crystalline structure impairs cell

formation, favoring cell coalescence and therefore forming larger pores [93]. However, this phenomenon is not seen in the PLA(4)/PBAT(84) polymer, where its crystallinity behaves in the same way when varying the pressure. This may be due to the fact that in the mixture of this polymer there is calcium carbonate, which can act as a stabilizer and act on the coalescence of foam cells independently of the crystallinity, which can also impact the drastic growth of cell density when foaming at 25 MPa [94].

Lower expansion rates can be seen when foams with IC are used, which may be due to the fact that the active agent interferes with the crystallinity of the polymers, leading to the formation of homogeneous cells that hinder the expansion rate [95]. Regarding the effect of pressure on the polymers, there is a tendency for the expansion rate to decrease as the pressure increases to 25 MPa with the exception of PLA(42)/PBAT(58) polymer, where the opposite behavior is observed. This phenomenon is related to the changes in crystallinity observed in the DSC analysis. Specially, a higher crystallinity percentage suggests a greater degree of molecular ordering, however, which in turn may hinder scCO₂ diffusion and bubble formation [96].

4. Conclusions

This study presents the characterization of PLA and PLA/PBAT films and foams impregnated with a caffeic acid/ β -cyclodextrin inclusion complex, focusing on their thermal, structural, and morphological properties. NMR, FTIR, and TGA analyses confirmed the successful inclusion of caffeic acid in β -cyclodextrin. Additionally, DSC analysis of the PLA and PLA/PBAT samples (both films and foams) further validated the incorporation of the inclusion complex through impregnation with scCO₂.

The foams previously impregnated with IC presented a lower loss of the active compound during the foaming process, it is related to the polarity of the external layer of the β -CD. This effect could be beneficial for obtaining a material with potential use in food packaging, with antioxidant activity without the need to impregnate a large amount of IC, since according to what has been reported, the molecular inclusion of this type of compound contributes to an increase in antioxidant activity.

Finally, serial impregnation and foaming allowed the production of materials with a variety of cell morphologies. This versatility of the process is explained by several factors related to supercritical CO₂ desorption and expansion, such as the chemical nature of the active agent, the physicochemical and transport properties of both polymers and their different mechanical properties.

Author Contributions: Conceptualization, A.T.; Data curation, F.R.-M. and J.B.; Formal analysis, P.R., M.P. and M.P.A.; Investigation, M.P.; Resources, J.R.; Supervision, A.T. and J.R.; Writing—original draft, P.R. and M.P.A.; Writing—review and editing, F.R.-M. and J.B. All authors have read and agreed to the published version of the manuscript.

Funding: This research was funded by projects from ANID FONDECYT No. 1221219 and 1230795. The authors thank the University of Santiago de Chile for the financial support of DICYT Project 082271TM_DAS. Patricia Rivera thanks the National Commission for Scientific and Technological Research, ANID, for the financial support of the National Doctoral Scholarship (Grant Number 21221075) and the Vicerrectoría de Postgrado of the University of Santiago de Chile for the support scholarship. The authors thank the financial support of CEDENNA, the Spanish Ministry of Science and Innovation (MICINN) through the PID-AEI Project (Grant PID2021-123753NA-C32) and the Research Consolidation Project (Grant CNS2022-136064) funded by MCIN/AEI/10.13039/501100011033 and by the ERDF “A way of making Europe” through the “European Union NextGenerationEU/PRTR”.

Institutional Review Board Statement: Not applicable.

Data Availability Statement: The data presented in this study are available upon request from the corresponding authors (due to privacy).

Acknowledgments: The authors thank the staff of the Laboratory of Membrane Separation Processes (LabProSeM), University of Santiago, Chile (USACH), for their assistance with the supercritical system.

Conflicts of Interest: The authors declare no conflicts of interest.

References

- Okolieocha, C.; Raps, D.; Subramaniam, K.; Altstädt, V. Microcellular to Nanocellular Polymer Foams: Progress (2004–2015) and Future Directions—A Review. *Eur. Polym. J.* **2015**, *73*, 500–519. [[CrossRef](#)]
- Desole, M.P.; Gisario, A.; Fedele, L.; Aversa, C.; Barletta, M. Life Cycle Assessment of Secondary Packaging: Expanded Polystyrene versus Bioplastic-Coated Corrugated Cardboard. *Sustain. Prod. Consum.* **2024**, *46*, 11–28. [[CrossRef](#)]
- Ghasemlou, M.; Barrow, C.J.; Adhikari, B. The Future of Bioplastics in Food Packaging: An Industrial Perspective. *Food Packag. Shelf Life* **2024**, *43*, 101279. [[CrossRef](#)]
- Ingrao, C.; Lo Giudice, A.; Bacenetti, J.; Mousavi Khaneghah, A.; Sant’Ana, A.S.; Rana, R.; Siracusa, V. Foamy Polystyrene Trays for Fresh-Meat Packaging: Life-Cycle Inventory Data Collection and Environmental Impact Assessment. *Food Res. Int.* **2015**, *76*, 418–426. [[CrossRef](#)]
- Parker, K.; Garancher, J.-P.; Shah, S.; Fernyhough, A. Expanded Polylactic Acid—An Eco-Friendly Alternative to Polystyrene Foam. *J. Cell. Plast.* **2011**, *47*, 233–243. [[CrossRef](#)]
- Chai, J.; Wang, G.; Zhao, J.; Zhang, A.; Shi, Z.; Wei, C.; Zhao, G. Microcellular PLA/PMMA Foam Fabricated by CO₂ foaming with Outstanding Shape-Memory Performance. *J. CO₂ Util.* **2021**, *49*, 101553. [[CrossRef](#)]
- Miranda-Valdez, I.Y.; Coffeng, S.; Zhou, Y.; Viitanen, L.; Hu, X.; Jannuzzi, L.; Puisto, A.; Kostianen, M.A.; Mäkinen, T.; Koivisto, J.; et al. Foam-Formed Biocomposites Based on Cellulose Products and Lignin. *Cellulose* **2023**, *30*, 2253–2266. [[CrossRef](#)]
- Nechita, P.; Năstac, S.M. Overview on Foam Forming Cellulose Materials for Cushioning Packaging Applications. *Polymers* **2022**, *14*, 1963. [[CrossRef](#)]
- Nofar, M.; Park, C.B. Poly (Lactic Acid) Foaming. *Prog. Polym. Sci.* **2014**, *39*, 1721–1741. [[CrossRef](#)]
- Oluwabunmi, K.; D’Souza, N.A.; Zhao, W.; Choi, T.Y.; Theyson, T. Compostable, Fully Biobased Foams Using PLA and Micro Cellulose for Zero Energy Buildings. *Sci. Rep.* **2020**, *10*, 17771. [[CrossRef](#)]
- Díez-Pascual, A.M. Biopolymer Composites: Synthesis, Properties, and Applications. *Int. J. Mol. Sci.* **2022**, *23*, 2257. [[CrossRef](#)] [[PubMed](#)]
- de Souza, F.M.; Desai, Y.; Gupta, R.K. Introduction to Polymeric Foams. In *ACS Symposium Series*; American Chemical Society: Washington, DC, USA, 2023; Volume 1439, pp. 1–23.
- Li, L.; Xu, D.; Bai, S.; Chen, N.; Wang, Q. Progress in Preparation of High-performance and Multi-functional Polymer Foams. *J. Polym. Sci.* **2024**, *62*, 3122–3136. [[CrossRef](#)]
- Osman, M.A.; Virgilio, N.; Rouabhia, M.; Mighri, F. Polylactic Acid (PLA) Foaming: Design of Experiments for Cell Size Control. *Mater. Sci. Appl.* **2022**, *13*, 63–77. [[CrossRef](#)]
- Li, Q.; Li, Q.; Cao, H.; Wu, J.; Wang, F.; Wang, Y. The Crack Propagation Behaviour of CO₂ Fracturing Fluid in Unconventional Low Permeability Reservoirs: Factor Analysis and Mechanism Revelation. *Processes* **2025**, *13*, 159. [[CrossRef](#)]
- Li, Q.; Li, Q.; Wu, J.; Li, X.; Li, H.; Cheng, Y. Wellhead Stability During Development Process of Hydrate Reservoir in the Northern South China Sea: Evolution and Mechanism. *Processes* **2024**, *13*, 40. [[CrossRef](#)]
- Chang, C.J.; Venkatesan, M.; Cho, C.J.; Chung, P.Y.; Chandrasekar, J.; Lee, C.H.; Wang, H.T.; Wong, C.M.; Kuo, C.C. Thermoplastic Starch with Poly(Butylene Adipate-Co-Terephthalate) Blends Foamed by Supercritical Carbon Dioxide. *Polymers* **2022**, *14*, 1952. [[CrossRef](#)] [[PubMed](#)]
- Faba, S.; Arrieta, M.P.; Romero, J.; Agüero, Á.; Torres, A.; Martínez, S.; Rayón, E.; Galotto, M.J. Biodegradable Nanocomposite Poly(Lactic Acid) Foams Containing Carvacrol-Based Cocrystal Prepared by Supercritical CO₂ Processing for Controlled Release in Active Food Packaging. *Int. J. Biol. Macromol.* **2024**, *254*, 127793. [[CrossRef](#)]
- Dejene, B.K.; Gudayu, A.D. Eco-Friendly Packaging Innovations: Integrating Natural Fibers and ZnO Nanofillers in Polylactic Acid (PLA) Based Green Composites—A Review. *Polym.-Plast. Technol. Mater.* **2024**, *63*, 1645–1681. [[CrossRef](#)]
- Westlake, J.R.; Tran, M.W.; Jiang, Y.; Zhang, X.; Burrows, A.D.; Xie, M. Biodegradable Biopolymers for Active Packaging: Demand, Development and Directions. *Sustain. Food Technol.* **2023**, *1*, 50–72. [[CrossRef](#)]
- Kaczmarek-Szczepańska, B.; Sosik, A.; Małkowska, A.; Zasada, L.; Michalska-Sionkowska, M. Chitosan-Based Films Enriched by Caffeic Acid with Poly(Ethylene Glycol)—A Physicochemical and Antibacterial Properties Evaluation. *Int. J. Biol. Macromol.* **2021**, *192*, 728–735. [[CrossRef](#)]

22. Wang, Y.; Du, H.; Xie, M.; Ma, G.; Yang, W.; Hu, Q.; Pei, F. Characterization of the Physical Properties and Biological Activity of Chitosan Films Grafted with Gallic Acid and Caffeic Acid: A Comparison Study. *Food Packag. Shelf Life* **2019**, *22*, 100401. [[CrossRef](#)]
23. Luzi, F.; Torre, L.; Puglia, D. Antioxidant Packaging Films Based on Ethylene Vinyl Alcohol Copolymer (EVOH) and Caffeic Acid. *Molecules* **2020**, *25*, 3953. [[CrossRef](#)]
24. Wang, Z.-Q.; Song, Q.-Y.; Su, J.-C.; Tang, W.; Song, J.-G.; Huang, X.-J.; An, J.; Li, Y.-L.; Ye, W.-C.; Wang, Y. Caffeic Acid Oligomers from *Mesona Chinensis* and Their In Vitro Antiviral Activities. *Fitoterapia* **2020**, *144*, 104603. [[CrossRef](#)]
25. Yu, S.-H.; Hsieh, H.-Y.; Pang, J.-C.; Tang, D.-W.; Shih, C.-M.; Tsai, M.-L.; Tsai, Y.-C.; Mi, F.-L. Active Films from Water-Soluble Chitosan/Cellulose Composites Incorporating Releasable Caffeic Acid for Inhibition of Lipid Oxidation in Fish Oil Emulsions. *Food Hydrocoll.* **2013**, *32*, 9–19. [[CrossRef](#)]
26. Zhang, M.; Li, J.; Zhang, L.; Chao, J. Preparation and Spectral Investigation of Inclusion Complex of Caffeic Acid with Hydroxypropyl- β -Cyclodextrin. *Spectrochim. Acta A Mol. Biomol. Spectrosc.* **2009**, *71*, 1891–1895. [[CrossRef](#)]
27. Pei, F.; Han, P.; Zhou, Z.; Fang, D.; Mariga, A.M.; Yang, W.; Ma, N.; Hu, Q. The Characteristics of the Film Assembled by Caffeic Acid-Grafted-Chitosan/Poly(lactic Acid) and Its Effect on the Postharvest Quality of *Agaricus Bisporus*. *Food Packag. Shelf Life* **2022**, *32*, 100828. [[CrossRef](#)]
28. Kfoury, M.; Hădăruță, N.G.; Hădăruță, D.I.; Fourmentin, S. Cyclodextrins as Encapsulation Material for Flavors and Aroma. In *Encapsulations*; Elsevier: Amsterdam, The Netherlands, 2016; pp. 127–192. ISBN 9780128043073.
29. Zhu, Y.; Li, C.; Cui, H.; Lin, L. Encapsulation Strategies to Enhance the Antibacterial Properties of Essential Oils in Food System. *Food Control.* **2021**, *123*, 107856. [[CrossRef](#)]
30. Faba, S.; Arrieta, M.P.; Agüero, Á.; Torres, A.; Romero, J.; Rojas, A.; Galotto, M.J. Processing Compostable PLA/Organoclay Bionanocomposite Foams by Supercritical CO₂ Foaming for Sustainable Food Packaging. *Polymers* **2022**, *14*, 4394. [[CrossRef](#)]
31. Klinmalai, P.; Srisa, A.; Laurenza, Y.; Katekhong, W.; Harnkarnsujarit, N. Antifungal and Plasticization Effects of Carvacrol in Biodegradable Poly(Lactic Acid) and Poly(Butylene Adipate Terephthalate) Blend Films for Bakery Packaging. *LWT* **2021**, *152*, 112356. [[CrossRef](#)]
32. Lopresti, F.; Botta, L.; Scaffaro, R.; Bilello, V.; Settanni, L.; Gaglio, R. Antibacterial Biopolymeric Foams: Structure–Property Relationship and Carvacrol Release Kinetics. *Eur. Polym. J.* **2019**, *121*, 109298. [[CrossRef](#)]
33. Christaki, S.; Spanidi, E.; Panagiotidou, E.; Athanasopoulou, S.; Kyriakoudi, A.; Mourtzinos, I.; Gardikis, K. Cyclodextrins for the Delivery of Bioactive Compounds from Natural Sources: Medicinal, Food and Cosmetics Applications. *Pharmaceuticals* **2023**, *16*, 1274. [[CrossRef](#)] [[PubMed](#)]
34. da Silva, W.F.; dos Santos Niculau, E.; de Oliveira, D.A.B.; de Assis, M.W.V.; Oliveira, M.N. Preparation, Physicochemical Characterization and Computational Studies of *Plectranthus Ornatus* Codd Essential Oil/ β -Cyclodextrin Inclusion Complex. *J. Mol. Struct.* **2023**, *1285*, 135476. [[CrossRef](#)]
35. Torres, L.H.; de Carvalho, M.Z.; Melo, P.S.; de Paula, E.; Saczk, A.A.; Pinto, L.M.A. Characterization and Cytotoxicity of a Benzocaine Inclusion Complex. *J. Incl. Phenom. Macrocycl. Chem.* **2018**, *91*, 9–15. [[CrossRef](#)]
36. Zhao, Y.; Zhu, B.; Wang, Y.; Liu, C.; Shen, C. Effect of Different Sterilization Methods on the Properties of Commercial Biodegradable Polyesters for Single-Use, Disposable Medical Devices. *Mater. Sci. Eng. C* **2019**, *105*, 110041. [[CrossRef](#)] [[PubMed](#)]
37. Scaffaro, R.; Maio, A.; Gammino, M.; La Mantia, F.P. Effect of an Organoclay on the Photochemical Transformations of a PBAT/PLA Blend and Morpho-Chemical Features of Crosslinked Networks. *Polym. Degrad. Stab.* **2021**, *187*, 109549. [[CrossRef](#)]
38. Muñoz-Shugulí, C.; Rodríguez-Mercado, F.; Mascayano, C.; Herrera, A.; Bruna, J.E.; Guarda, A.; Galotto, M.J. Development of Inclusion Complexes With Relative Humidity Responsive Capacity as Novel Antifungal Agents for Active Food Packaging. *Front. Nutr.* **2022**, *8*, 799779. [[CrossRef](#)]
39. Torres, A.; Ilabaca, E.; Rojas, A.; Rodríguez, F.; Galotto, M.J.; Guarda, A.; Villegas, C.; Romero, J. Effect of Processing Conditions on the Physical, Chemical and Transport Properties of Poly(lactic Acid) Films Containing Thymol Incorporated by Supercritical Impregnation. *Eur. Polym. J.* **2017**, *89*, 195–210. [[CrossRef](#)]
40. Mistretta, M.C.; La Mantia, F.P.; Titone, V.; Botta, L.; Pedferri, M.; Morreale, M. Effect of Ultraviolet and Moisture Action on Biodegradable Polymers and Their Blend. *J. Appl. Biomater. Funct. Mater.* **2020**, *18*, 228080002092665. [[CrossRef](#)]
41. Rivera, P.; Torres, A.; Romero, J.; Alarcón, Á.; Martínez, S.; Arrieta, M.P.; Rodríguez-Mercado, F.; Galotto, M.J. Effect of Operational Variables on Supercritical Foaming of Caffeic Acid-Loaded Poly(Lactic Acid)/Poly(Butylene Adipate-Co-Terephthalate) Blends for the Development of Sustainable Materials. *Polymers* **2024**, *16*, 948. [[CrossRef](#)]
42. Nofar, M.; Tabatabaei, A.; Sojoudiasli, H.; Park, C.B.; Carreau, P.J.; Heuzey, M.C.; Kamal, M.R. Mechanical and Bead Foaming Behavior of PLA-PBAT and PLA-PBSA Blends with Different Morphologies. *Eur. Polym. J.* **2017**, *90*, 231–244. [[CrossRef](#)]
43. Arrua, D.; Strumia, M.C.; Nazareno, M.A. Immobilization of Caffeic Acid on a Polypropylene Film: Synthesis and Antioxidant Properties. *J. Agric. Food Chem.* **2010**, *58*, 9228–9234. [[CrossRef](#)] [[PubMed](#)]

44. Menezes, P.d.P.; Serafini, M.R.; de Carvalho, Y.M.B.G.; Soares Santana, D.V.; Lima, B.S.; Quintans-Júnior, L.J.; Marreto, R.N.; de Aquino, T.M.; Sabino, A.R.; Scotti, L.; et al. Kinetic and Physical-Chemical Study of the Inclusion Complex of β -Cyclodextrin Containing Carvacrol. *J. Mol. Struct.* **2016**, *1125*, 323–330. [[CrossRef](#)]
45. Weigend, F.; Ahlrichs, R.; Gmbh, F.K. Balanced Basis Sets of Split Valence, Triple Zeta Valence and Quadruple Zeta Valence Quality for H to Rn: Design and Assessment of Accuracy. *Phys. Chem. Chem. Phys.* **2005**, *7*, 3297. [[CrossRef](#)]
46. Kuska, R.; Milovanovic, S.; Frerich, S.; Ivanovic, J. Thermal Analysis of Polylactic Acid under High CO₂ Pressure Applied in Supercritical Impregnation and Foaming Process Design. *J. Supercrit. Fluids* **2019**, *144*, 71–80. [[CrossRef](#)]
47. ASTM D792; Test Methods for Density and Specific Gravity (Relative Density) of Plastics by Displacement. ASTM International: West Conshohocken, PA, USA, 2020.
48. Pilla, S.; Kim, S.G.; Auer, G.K.; Gong, S.; Park, C.B. Microcellular Extrusion Foaming of Poly(Lactide)/Poly(Butylene Adipate-Co-Terephthalate) Blends. *Mater. Sci. Eng. C* **2010**, *30*, 255–262. [[CrossRef](#)] [[PubMed](#)]
49. Liu, W.; Chen, P.; Wang, X.; Wang, F.; Wu, Y. Effects of Poly(Butyleneadipate-Co-Terephthalate) as a Macromolecular Nucleating Agent on the Crystallization and Foaming Behavior of Biodegradable Poly(Lactic Acid). *Cell. Polym.* **2017**, *36*, 75–96. [[CrossRef](#)]
50. Kalogeropoulos, N.; Konteles, S.; Mourtzinis, I.; Troullidou, E.; Chiou, A.; Karathanos, V.T. Encapsulation of Complex Extracts in β -Cyclodextrin: An Application to Propolis Ethanolic Extract. *J. Microencapsul.* **2009**, *26*, 603–613. [[CrossRef](#)]
51. Chao, J.-B.; Tong, H.-B.; Li, Y.-F.; Zhang, L.-W.; Zhang, B.-T. Investigation on the Inclusion Behavior of Caffeic Acid with Cyclodextrin. *Supramol. Chem.* **2008**, *20*, 461–466. [[CrossRef](#)]
52. Pinho, E.; Soares, G.; Henriques, M. Evaluation of Antibacterial Activity of Caffeic Acid Encapsulated by β -Cyclodextrins. *J. Microencapsul.* **2015**, *32*, 804–810. [[CrossRef](#)]
53. Kfoury, M.; Geagea, C.; Ruellan, S.; Greige-Gerges, H.; Fourmentin, S. Effect of Cyclodextrin and Cosolvent on the Solubility and Antioxidant Activity of Caffeic Acid. *Food Chem.* **2019**, *278*, 163–169. [[CrossRef](#)]
54. Herrera, A.; Rodríguez, F.J.; Bruna, J.E.; Abarca, R.L.; Galotto, M.J.; Guarda, A.; Mascayano, C.; Sandoval-Yáñez, C.; Padula, M.; Felipe, F.R.S. Antifungal and Physicochemical Properties of Inclusion Complexes Based on β -Cyclodextrin and Essential Oil Derivatives. *Food Res. Int.* **2019**, *121*, 127–135. [[CrossRef](#)] [[PubMed](#)]
55. Shiozawa, R.; Inoue, Y.; Murata, I.; Kanamoto, I. Effect of Antioxidant Activity of Caffeic Acid with Cyclodextrins Using Ground Mixture Method. *Asian J. Pharm. Sci.* **2018**, *13*, 24–33. [[CrossRef](#)] [[PubMed](#)]
56. Simsek, T.; Simsek, S.; Mayer, C.; Rasulev, B. Combined Computational and Experimental Study on the Inclusion Complexes of β -Cyclodextrin with Selected Food Phenolic Compounds. *Struct. Chem.* **2019**, *30*, 1395–1406. [[CrossRef](#)]
57. Narayanan, V.; Alam, M.; Ahmad, N.; Balakrishnan, S.B.; Ganesan, V.; Shanmugasundaram, E.; Rajagopal, B.; Thambusamy, S. Electrospun Poly (Vinyl Alcohol) Nanofibers Incorporating Caffeic Acid/Cyclodextrins through the Supramolecular Assembly for Antibacterial Activity. *Spectrochim. Acta A Mol. Biomol. Spectrosc.* **2021**, *249*, 119308. [[CrossRef](#)]
58. Trindade, G.G.G.; Thirvikraman, G.; Menezes, P.P.; França, C.M.; Lima, B.S.; Carvalho, Y.M.B.G.; Souza, E.P.B.S.S.; Duarte, M.C.; Shanmugam, S.; Quintans-Júnior, L.J.; et al. Carvacrol/ β -Cyclodextrin Inclusion Complex Inhibits Cell Proliferation and Migration of Prostate Cancer Cells. *Food Chem. Toxicol.* **2019**, *125*, 198–209. [[CrossRef](#)] [[PubMed](#)]
59. Zhang, X.; Su, J.; Wang, X.; Wang, X.; Liu, R.; Fu, X.; Li, Y.; Xue, J.; Li, X.; Zhang, R.; et al. Preparation and Properties of Cyclodextrin Inclusion Complexes of Hyperoside. *Molecules* **2022**, *27*, 2761. [[CrossRef](#)]
60. Mangrulkar, S.; Shah, P.; Navnage, S.; Mazumdar, P.; Chaple, D. Phytophospholipid Complex of Caffeic Acid: Development, In Vitro Characterization, and In Vivo Investigation of Antihyperlipidemic and Hepatoprotective Action in Rats. *AAPS PharmSciTech* **2021**, *22*, 28. [[CrossRef](#)]
61. Li, R.; Bao, R.; Yang, Q.X.; Wang, Q.L.; Adu-Frimpong, M.; Wei, Q.Y.; Elmurat, T.; Ji, H.; Yu, J.N.; Xu, X.M. [6]-Shogaol/ β -CDs Inclusion Complex: Preparation, Characterisation, in Vivo Pharmacokinetics, and in Situ Intestinal Perfusion Study. *J. Microencapsul.* **2019**, *36*, 500–512. [[CrossRef](#)]
62. Abarca, R.L.; Rodríguez, F.J.; Guarda, A.; Galotto, M.J.; Bruna, J.E. Characterization of Beta-Cyclodextrin Inclusion Complexes Containing an Essential Oil Component. *Food Chem.* **2016**, *196*, 968–975. [[CrossRef](#)]
63. Zeren, S.; Sahin, S.; Sumnu, G. Encapsulation of Caffeic Acid in Carob Bean Flour and Whey Protein-Based Nanofibers via Electrospinning. *Foods* **2022**, *11*, 1860. [[CrossRef](#)]
64. Sambasevam, K.; Mohamad, S.; Sarih, N.; Ismail, N. Synthesis and Characterization of the Inclusion Complex of β -Cyclodextrin and Azomethine. *Int. J. Mol. Sci.* **2013**, *14*, 3671–3682. [[CrossRef](#)] [[PubMed](#)]
65. Gupta, R.B.; Shim, J.-J. *Solubility in Supercritical Carbon Dioxide*; CRC Press: Boca Raton, FL, USA, 2006; ISBN 9780429122088.
66. Bitencourt, R.G.; Palma, A.M.; Coutinho, J.A.P.; Cabral, F.A.; Meirelles, A.J.A. Solubility of Caffeic Acid in CO₂+ ethanol: Experimental and Predicted Data Using Cubic Plus Association Equation of State. *J. Supercrit. Fluids* **2018**, *138*, 238–246. [[CrossRef](#)]
67. Shi, X.; Qin, J.; Wang, L.; Ren, L.; Rong, F.; Li, D.; Wang, R.; Zhang, G. Introduction of Stereocomplex Crystallites of PLA for the Solid and Microcellular Poly(Lactide)/Poly(Butylene Adipate- Co-Terephthalate) Blends. *RSC Adv.* **2018**, *8*, 11850–11861. [[CrossRef](#)] [[PubMed](#)]

68. Cejudo Bastante, C.; Casas Cardoso, L.; Fernández-Ponce, M.T.; Mantell Serrano, C.; Martínez de la Ossa, E.J. Supercritical Impregnation of Olive Leaf Extract to Obtain Bioactive Films Effective in Cherry Tomato Preservation. *Food Packag. Shelf Life* **2019**, *21*, 100338. [[CrossRef](#)]
69. Rojas, A.; Cerro, D.; Torres, A.; Galotto, M.J.; Guarda, A.; Romero, J. Supercritical Impregnation and Kinetic Release of 2-Nonanone in LLDPE Films Used for Active Food Packaging. *J. Supercrit. Fluids* **2015**, *104*, 76–84. [[CrossRef](#)]
70. Milovanovic, S.; Hollermann, G.; Errenst, C.; Pajnik, J.; Frerich, S. Supercritical CO₂ Impregnation of PLA / PCL Films with Natural Substances for Bacterial Growth Control in Food Packaging. *Food Res. Int.* **2018**, *107*, 486–495. [[CrossRef](#)] [[PubMed](#)]
71. de Souza, A.C.; Dias, A.M.A.; Sousa, H.C.; Tadini, C.C. Impregnation of Cinnamaldehyde into Cassava Starch Biocomposite Films Using Supercritical Fluid Technology for the Development of Food Active Packaging. *Carbohydr. Polym.* **2014**, *102*, 830–837. [[CrossRef](#)]
72. Machado, N.D.; Mosquera, J.E.; Martini, R.E.; Goñi, M.L.; Gañán, N.A. Supercritical CO₂-Assisted Impregnation/Deposition of Polymeric Materials with Pharmaceutical, Nutraceutical, and Biomedical Applications: A Review (2015–2021). *J. Supercrit. Fluids* **2022**, *191*, 105763. [[CrossRef](#)]
73. Da Silva, C.V.; Pereira, V.J.; Rosa, P.T.V.; Cabral-Albuquerque, E.C.M.; Vieira De Melo, S.A.B.; Costa, G.M.N.; Dias, A.M.A.; De Sousa, H.C.; Braga, M.E.M. Effect of ScCO₂ Sorption Capacity on the Total Amount of Borage Oil Loaded by ScCO₂ Impregnation/Deposition into a Polyurethane-Based Wound Dressing. *J. Supercrit. Fluids* **2016**, *115*, 1–9. [[CrossRef](#)]
74. Pai, A.J.; Sarojini, B.K.; Harshitha, K.R.; Shivarama Holla, B.; Lobo, A.G. Spectral, Morphological and Optical Studies on Bischalcone Doped Poly(lactic Acid) (PLA) Thin Films as Luminescent and UV Radiation Blocking Materials. *Opt. Mater.* **2019**, *90*, 145–151. [[CrossRef](#)]
75. Moliner, C.; Finocchio, E.; Arato, E.; Ramis, G.; Lagazzo, A. Influence of the Degradation Medium on Water Uptake, Morphology, and Chemical Structure of Poly(Lactic Acid)-Sisal Bio-Composites. *Materials* **2020**, *13*, 3974. [[CrossRef](#)]
76. Ramezani, M.; Amoozegar, M.A.; Ventosa, A. Screening and Comparative Assay of Poly-Hydroxyalkanoates Produced by Bacteria Isolated from the Gavkhoni Wetland in Iran and Evaluation of Poly-β-Hydroxybutyrate Production by Halotolerant Bacterium *Oceanimonas* sp. GK1. *Ann. Microbiol.* **2015**, *65*, 517–526. [[CrossRef](#)]
77. Villegas, C.; Torres, A.; Rios, M.; Rojas, A.; Romero, J.; de Dicastillo, C.L.; Valenzuela, X.; Galotto, M.J.; Guarda, A. Supercritical Impregnation of Cinnamaldehyde into Poly(lactic Acid) as a Route to Develop Antibacterial Food Packaging Materials. *Food Res. Int.* **2017**, *99*, 650–659. [[CrossRef](#)] [[PubMed](#)]
78. Nunes, F.C.; Ribeiro, K.C.; Martini, F.A.; Barrioni, B.R.; Santos, J.P.F.; Melo Carvalho, B. PBAT/PLA/Cellulose Nanocrystals Biocomposites Compatibilized with Polyethylene Grafted Maleic Anhydride (PE-g-MA). *J. Appl. Polym. Sci.* **2021**, *138*, 151342. [[CrossRef](#)]
79. Meaurio, E.; López-Rodríguez, N.; Sarasua, J.R. Infrared Spectrum of Poly(L-Lactide): Application to Crystallinity Studies. *Macromolecules* **2006**, *39*, 9291–9301. [[CrossRef](#)]
80. Cejudo Bastante, C.; Cran, M.J.; Casas Cardoso, L.; Mantell Serrano, C.; Martínez de la Ossa, E.J.; Bigger, S.W. Effect of Supercritical CO₂ and Olive Leaf Extract on the Structural, Thermal and Mechanical Properties of an Impregnated Food Packaging Film. *J. Supercrit. Fluids* **2019**, *145*, 181–191. [[CrossRef](#)]
81. Ma, F.; Wang, B.; Leng, X.; Wang, Y.; Sun, Z.; Wang, P.; Sang, L.; Wei, Z. Biodegradable PBAT/PLA/CaCO₃ Blowing Films with Enhanced Mechanical and Barrier Properties: Investigation of Size and Content of CaCO₃ Particles. *Macromol. Mater. Eng.* **2022**, *307*, 2200135. [[CrossRef](#)]
82. Rocha, D.B.; Souza de Carvalho, J.; de Oliveira, S.A.; dos Santos Rosa, D. A New Approach for Flexible PBAT/PLA/CaCO₃ Films into Agriculture. *J. Appl. Polym. Sci.* **2018**, *135*, 1–9. [[CrossRef](#)]
83. Teamsinsungvon, A.; Jarapanyacheep, R.; Ruksakulpiwat, Y.; Jarukumjorn, K. Melt Processing of Maleic Anhydride Grafted Poly(Lactic Acid) and Its Compatibilizing Effect on Poly(Lactic Acid)/Poly(Butylene Adipate-Co-Terephthalate) Blend and Their Composite. *Polym. Sci. Ser. A* **2017**, *59*, 384–396. [[CrossRef](#)]
84. Chiu, H.-T.; Huang, S.-Y.; Chen, Y.-F.; Kuo, M.-T.; Chiang, T.-Y.; Chang, C.-Y.; Wang, Y.-H. Heat Treatment Effects on the Mechanical Properties and Morphologies of Poly (Lactic Acid)/Poly (Butylene Adipate-Co-Terephthalate) Blends. *Int. J. Polym. Sci.* **2013**, *2013*, 951696. [[CrossRef](#)]
85. Shi, X.; Zhang, G.; Liu, Y.; Ma, Z.; Jing, Z.; Fan, X. Microcellular Foaming of Poly(lactide) and Poly(Butylene Adipate-co-terephthalate) Blends and Their CaCO₃ Reinforced Nanocomposites Using Supercritical Carbon Dioxide. *Polym. Adv. Technol.* **2016**, *27*, 550–560. [[CrossRef](#)]
86. Yang, Z.; Peng, H.; Wang, W.; Liu, T. Crystallization Behavior of Poly(ε-Caprolactone)/Layered Double Hydroxide Nanocomposites. *J. Appl. Polym. Sci.* **2010**, *116*, 2658–2667. [[CrossRef](#)]
87. Phetwarotai, W.; Tanrattanakul, V.; Phusunti, N. Mechanical Characteristics and Thermal Behaviours of Poly(lactide) Blend Films: Influence of Nucleating Agent and Poly(Butylenes Adipate-Co-Terephthalate). *Plast. Rubber Compos.* **2016**, *45*, 333–345. [[CrossRef](#)]
88. Byun, Y.; Rodriguez, K.; Han, J.H.; Kim, Y.T. Improved Thermal Stability of Poly(lactic Acid) (PLA) Composite Film via PLA-β-Cyclodextrin-Inclusion Complex Systems. *Int. J. Biol. Macromol.* **2015**, *81*, 591–598. [[CrossRef](#)]

89. Hao, A.; Geng, Y.; Xu, Q.; Lu, Z.; Yu, L. Study of Different Effects on Foaming Process of Biodegradable PLA/Starch Composites in Supercritical/Compressed Carbon Dioxide. *J. Appl. Polym. Sci.* **2008**, *109*, 2679–2686. [[CrossRef](#)]
90. Zhang, L.; Zhen, W.; Zhou, Y. Structure and Properties of Poly(Lactic Acid)/Poly(Lactic Acid)- α -Cyclodextrin Inclusion Compound Composites. *J. Polym. Eng.* **2017**, *37*, 897–909. [[CrossRef](#)]
91. Wang, J.; Chai, J.; Wang, G.; Zhao, J.; Zhang, D.; Li, B.; Zhao, H.; Zhao, G. Strong and Thermally Insulating Polylactic Acid/Glass Fiber Composite Foam Fabricated by Supercritical Carbon Dioxide Foaming. *Int. J. Biol. Macromol.* **2019**, *138*, 144–155. [[CrossRef](#)] [[PubMed](#)]
92. Milovanovic, S.; Markovic, D.; Mrakovic, A.; Kuska, R.; Zizovic, I.; Frerich, S.; Ivanovic, J. Supercritical CO₂—Assisted Production of PLA and PLGA Foams for Controlled Thymol Release. *Mater. Sci. Eng. C* **2019**, *99*, 394–404. [[CrossRef](#)]
93. Wang, Y.; Chen, S.; Mi, J.; Du, Z.; Wang, X.; Zhang, C. Effect of the Crystallization of Modified Polybutylene Terephthalate on Its Foaming Using Supercritical CO₂: Transition from Microcellular to Nanocellular Foam. *J. Supercrit. Fluids* **2022**, *181*, 105463. [[CrossRef](#)]
94. Moo-Tun, N.M.; Iñiguez-Covarrubias, G.; Valadez-Gonzalez, A. Assessing the Effect of PLA, Cellulose Microfibers and CaCO₃ on the Properties of Starch-Based Foams Using a Factorial Design. *Polym. Test.* **2020**, *86*, 106482. [[CrossRef](#)]
95. Liu, W.; Wu, X.; Chen, X.; Liu, S.; Zhang, C. Flexibly Controlling the Polycrystallinity and Improving the Foaming Behavior of Polylactic Acid via Three Strategies. *ACS Omega* **2022**, *7*, 6248–6260. [[CrossRef](#)] [[PubMed](#)]
96. Rezvanpanah, E.; Ghaffarian Anbaran, S.R. The Effect of Crystallinity on Cell Growth in Semi-Crystalline Microcellular Foams by Solid-State Process: Modeling and Numerical Simulation. *Mater. Res. Express* **2017**, *4*, 115305. [[CrossRef](#)]

Disclaimer/Publisher’s Note: The statements, opinions and data contained in all publications are solely those of the individual author(s) and contributor(s) and not of MDPI and/or the editor(s). MDPI and/or the editor(s) disclaim responsibility for any injury to people or property resulting from any ideas, methods, instructions or products referred to in the content.